Biogeosciences, 21, 5407–5433, 2024
https://doi.org/10.5194/bg-21-5407-2024
© Author(s) 2024. This work is distributed under
the Creative Commons Attribution 4.0 License.

Biogeosciences Open Access EGU

Characterizing regional oceanography and bottom environmental conditions at two contrasting sponge grounds on the northern Labrador Shelf

Evert de Froe[1,2,3], Igor Yashayaev[4], Christian Mohn[5], Johanne Vad[6], Furu Mienis[1], Gerard Duineveld[1], Ellen Kenchington[4], Erica Head[4], Steve W. Ross[7], Sabena Blackbird[8], George A. Wolff[8], J. Murray Roberts[6], Barry MacDonald[4], Graham Tulloch[9], and Dick van Oevelen[10]

[1]Department of Ocean Systems, NIOZ Royal Netherlands Institute for Sea Research, PO Box 59, 1790 AB Den Burg, the Netherlands
[2]Centre for Fisheries Ecosystems Research, Fisheries and Marine Institute of Memorial University of Newfoundland and Labrador, St. John's, NL A1C 5R3, Canada
[3]Wageningen Marine Research, Wageningen University and Research, PO Box 77, 4400 AB Yerseke, the Netherlands
[4]Department of Fisheries and Oceans, Bedford Institute of Oceanography, PO Box 1006, Dartmouth, NS B2Y 4A2, Canada
[5]Department of Ecoscience, Aarhus University, Frederiksborgvej 399, 4000 Roskilde, Denmark
[6]Changing Oceans Research Group, School of GeoSciences, The University of Edinburgh, Edinburgh, EH9 3FE, UK
[7]Center for Marine Science, University of North Carolina at Wilmington, 5600 Marvin Moss Ln., Wilmington, NC 28409, USA
[8]School of Environmental Sciences, University of Liverpool, 4 Brownlow Street, Liverpool, L69 3GP, UK
[9]Lyell Centre, British Geological Survey, Research Avenue South, Edinburgh, EH14 4AP, UK
[10]Department of Estuarine and Delta Systems, NIOZ Royal Netherlands Institute for Sea Research, PO Box 140, 4400 AC Yerseke, the Netherlands

Correspondence: Evert de Froe (evert.defroe@wur.nl)

Received: 30 January 2024 – Discussion started: 2 February 2024
Revised: 7 September 2024 – Accepted: 5 October 2024 – Published: 6 December 2024

Abstract. Deep-sea sponge grounds are distributed globally and are considered hotspots of biological diversity and biogeochemical cycling. To date, little is known about the environmental conditions that allow high sponge biomass to develop in the deep sea. Here, we characterize oceanographic conditions at two contrasting sites off the northern Labrador Shelf with respective high and low sponge biomass. Data were collected by year-long benthic lander deployments equipped with current meters, a turbidity and chlorophyll-*a* measuring device, and a sediment trap. Additionally, regional oceanography was described by analysing vertical conductivity–temperature–depth (CTD) casts, Argo float profiles, and surface buoy drifter data for the northern Labrador Shelf from 2005 to 2022. The stable isotopic composition of benthic fauna was determined to investigate food web structure at the sponge grounds. Our results revealed strong ($0.26 \pm 0.14\,m\,s^{-1}$; mean ± SD) semidiurnal tidal currents at the high-sponge-biomass site but 2-fold weaker currents ($0.14 \pm 0.08\,m\,s^{-1}$; mean ± SD) at the low-sponge-biomass site. Tidal analysis suggests that kinetic energy is dissipated from barotropic tide to baroclinic tide/turbulence at the high-sponge-biomass site, which could enhance food availability for benthic organisms. Bottom nutrient concentrations were elevated at the high-sponge-biomass site, which would benefit growth in deep-sea sponges. Organic matter flux to the seafloor was increased at the high-sponge-biomass site and consisted of fresher material. Finally, both sponge grounds demonstrated tight benthic–pelagic coupling prior to the onset of stratification. Stable isotope signatures indicated that soft corals (*Primnoa resedaeformis*) fed on suspended particulate organic matter, while massive sponges (*Geodia* spp.) likely utilized additional food sources. Our results imply that benthic fauna at the high-sponge-biomass site benefit from strong tidal currents, which increase the food supply,

Published by Copernicus Publications on behalf of the European Geosciences Union.

and favourable regional ocean currents, which increase the nutrient concentration in bottom waters.

1 Introduction

Sponges are an ancient group of sessile filter feeders capable of pumping large quantities of water through their bodies (Bergquist, 1978; Leys et al., 2011; Vogel, 1977), thereby exchanging significant amounts of particulate and dissolved organic matter and nutrients with the water column (e.g. van Duyl et al., 2008; Maldonado et al., 2012; Kahn et al., 2015; Rix et al., 2016). In the deep sea, sponges can form dense aggregations, known as sponge grounds, which are considered hotspots of macrofaunal diversity and abundance (Beazley et al., 2013; Buhl-Mortensen et al., 2010; Klitgaard, 1995; McIntyre et al., 2016), carbon and nutrient cycling (Cathalot et al., 2015; Kutti et al., 2013; Maldonado et al., 2020b), and benthic–pelagic coupling (Pile and Young, 2006). Sponge grounds form complex habitats that provide breeding grounds and shelter for (commercially important) fish, increasing demersal fish biomass and diversity (Brodnicke et al., 2023; Kenchington et al., 2013; Kutti et al., 2015; Meyer et al., 2019). Finally, they are often classified as Vulnerable Marine Ecosystems (VMEs), as defined by the Food and Agriculture Organization of the United Nations (Hogg et al., 2010).

Deep-sea sponge ecosystems are currently under threat from anthropogenic disturbances such as deep-water bottom trawling, deep-sea mining, and climate change. Pham et al. (2019) found that large quantities of sponges ($\sim 4\,\%$ of total stock) have been removed by bottom trawling from sponge grounds in the Flemish Cap region. Deep-sea sponges are especially vulnerable to bottom fishing due to their longevity and slow growth (Hogg et al., 2010; Leys and Lauzon, 1998). Benthic trawling reduces the density and diversity of deep-sea sponge grounds (Colaço et al., 2022; Morrison et al., 2020), and recovery of disturbed sponge habitats can take decades to centuries (Vieira et al., 2020). In addition, prolonged exposure to elevated concentrations of suspended sediments, e.g. due to deep-sea mining, could adversely affect deep-sea sponges (Wurz et al., 2021). Recent studies suggest that climate change also impacts deep-sea benthic fauna (Brito-Morales et al., 2020; Jorda et al., 2020). For example, modelling predicted that the suitable area for *Vazella pourtalesii* on the Scotian Shelf would increase 4-fold in the coming years due to the warming of colder waters around its current habitat (Beazley et al., 2021). Nevertheless, research on the effect of climate change on deep-sea sponges is still in its infancy, and a better understanding of the environmental conditions that favour sponge occurrence is needed to predict the effects of such change on sponge grounds.

In the past decades, research on deep-sea sponges has focused on their physiology and feeding behaviour (e.g. Leys and Lauzon, 1998; Yahel et al., 2007; Kahn et al., 2015; Robertson et al., 2017; Kazanidis et al., 2018; Maier et al., 2020a; Bart et al., 2021; de Kluijver et al., 2021) and on assessing their spatial distributions using habitat suitability models (Beazley et al., 2018; Howell et al., 2016; Knudby et al., 2013; Murillo et al., 2018). More recently, data on the environmental conditions in sponge ground regions have been gathered using long-term measurements from lander-mounted equipment. These data indicate that sponge grounds are commonly found in areas with internal waves (Davison et al., 2019) and comparatively strong tidal currents, which flush the seafloor with oxygen and nutrient-rich water, and with a high suspended particle matter load near the seabed (Hanz et al., 2021a, b; Roberts et al., 2018). In addition, sponges can alter the hydrodynamic conditions of the benthic boundary layer by increasing the bottom roughness, creating conditions favourable for larval recruitment and suspended particle deposition (Abelson and Denny, 1997; Culwick et al., 2020). These studies show that sponge grounds are found in areas with a variety of environmental conditions, but little is known of the mechanisms controlling their spatial distribution or what controls their biomass.

The Canadian Atlantic continental shelf breaks and upper slopes, including the northern Labrador Shelf, host extensive sponge grounds (Kenchington et al., 2010; Knudby et al., 2013). Sponge assemblages occur over a large depth range (200–2875 m) and are often aligned along depth contours with presumably similar environmental conditions (Murillo et al., 2012; Knudby et al., 2013). On the northern Labrador Shelf and upper slope, sponge assemblages consist mostly of *Geodia* spp. and glass (hexactinellid) sponges (Kenchington et al., 2010) but with locally variable sponge biomass. Therefore, this region provides a suitable setting to study which environmental conditions favour high sponge biomass and to provide insight into the factors that drive the spatial distribution of sponge assemblages on the eastern Canadian Shelf. Furthermore, research on the present environmental conditions on the seafloor is timely, as the Labrador Shelf region is one of the fastest warming large marine ecosystems globally ($\sim 1\,^{\circ}\mathrm{C}$ per decade; Belkin, 2009), and according to ensemble-based climate change prediction, critical water mass properties there, including temperature, particulate organic carbon, pH, and aragonite saturation, are likely to change substantially by 2100 (Puerta et al., 2020). Recent work on the Labrador Sea also shows that Arctic sea-ice melt can impact the hydrographic conditions in this region (Yashayaev, 2024). Therefore, analysis of the contemporary conditions provides a baseline or a benchmark for referencing future ocean and ecosystem conditions. This study presents a valuable reference dataset for the upper slope of the northern Labrador Shelf against which future changes could be evaluated.

To obtain a better understanding of the environmental conditions and ecosystem functioning of high- and low-sponge-biomass sites on the upper slope of the northern Labrador

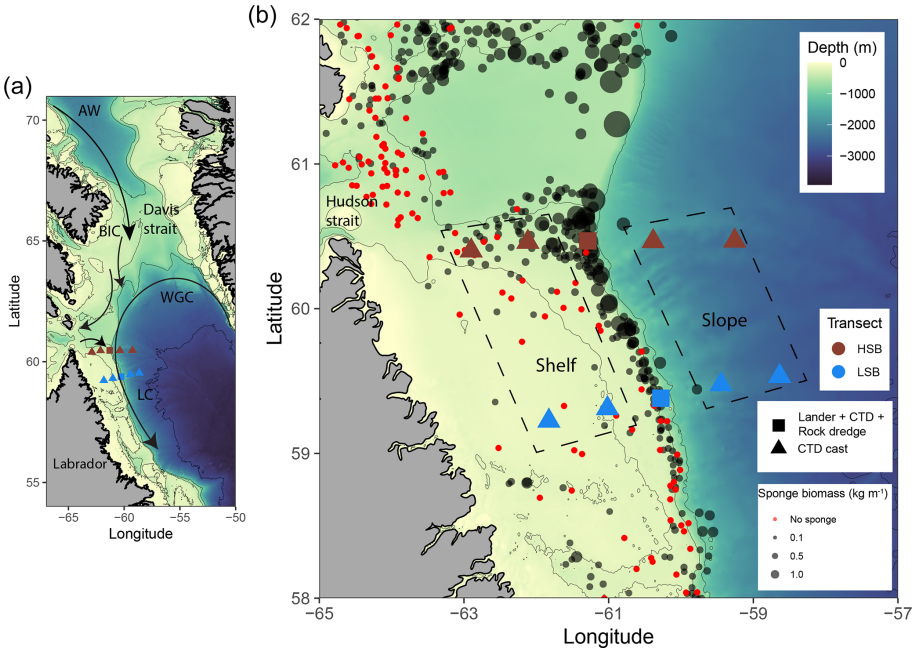

Figure 1. Map of the study area with **(a)** the general circulation pattern (Curry et al., 2014). Cold Artic Water (AW) flows southward through the Davis Strait and continues as the surface-intensified Baffin Island Current (BIC). The warmer, more saline West Greenland Current (WGC) of North Atlantic origin largely follows the continental slope in the depth range of 150–800 m and is deflected westward at approximately 64° N. Cold and fresh water leaves Hudson Strait and joins the BIC and WGC to form the offshore branch of the Labrador Current (Straneo and Saucier, 2008). **(b)** Location of lander deployments and CTD casts, with sponge biomass (in kg m^{-1}) based on Kenchington et al. (2010). Areas delineated with a dashed line indicate the shallow shelf and deeper slope stations (see panel labels) at both sites. HSB denotes the high-sponge-biomass transect (red symbols), whereas LSB denotes the low-sponge-biomass transect (blue symbols).

Shelf, this study specifically aimed to examine the following: (i) differences in ocean dynamics and seawater properties, (ii) the annual dynamics of near-bed environmental and hydrodynamic conditions, and (iii) differences in organic matter flux and isotopic signatures for sponges and associated macrofauna. To this end, data on regional oceanography of the northern Labrador Shelf were collected from conductivity–temperature–depth (CTD) casts, Argo float profiles, and surface drifter buoys. Bottom hydrodynamic- and environmental conditions were assessed using 2-year-long benthic lander deployments. Organic matter fluxes were measured with sediment traps, and benthic macrofauna was sampled by two rock dredge deployments. This study is the first to collect year-long hydrodynamic and environmental data simultaneously at a high- and a low-biomass sponge ground.

2 Material and methods

2.1 Oceanographic setting and the study area

The study area comprises the northern Labrador Shelf and upper slope and extends from the southeastern Hudson Strait outflow region to the base of the Labrador slope (Fig. 1a). This region is known for intense mixing and water mass transformation (Dunbar, 1951; Kollmeyer et al., 1967; Griffiths et al., 1981; Drinkwater and Jones, 1987), and four distinct flow components can be identified (Fig. 1a; Ricketts et al., 1931; Yashayaev, 2007; Straneo and Saucier, 2008; Curry et al., 2011, 2014): first, the cold and relatively fresh Arctic outflow, passing through the Davis Strait via the Baffin Island Current (BIC), enters the region from the north as Arctic Water (AW) and Baffin Bay Water (BBW; Sherwood et al., 2021); second, the West Greenland Current (WGC) approaches our study site from the northeast; third, Irminger Water (IW), a warmer and saltier water mass, can often be seen below the WGC, usually > 150 m depth; and fourth, Hudson Strait outflow water, which enters the region from the west. The resulting aggregated boundary current joins the Labrador Current (LC) flowing southward along the Labrador Shelf/slope, effectively forming and maintaining a baroclinic transition between the less-saline shelf water and the more-saline deep-basin water (Yashayaev, 2007).

The northern Labrador Shelf hosts multiple sponge grounds with a contrasting sponge community composition, density, and biomass (Dinn et al., 2020; Kenchington et al., 2010). We selected a high-sponge-biomass site (HSB; 410 m depth) in the north and a low-sponge-biomass site (LSB; 558 m depth) in the south of the study area (Fig. 1b; Table S1 in the Supplement), approximately 130 km apart. The sub-

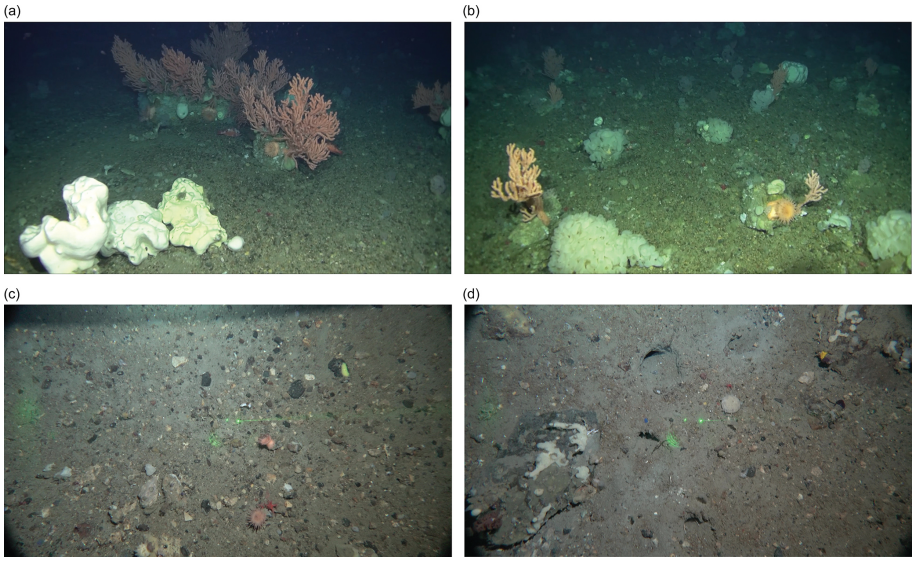

Figure 2. Images of benthic lander deployment sites, at the high-sponge-biomass (HSB) lander site (**a, b**) and low-sponge-biomass (LSB) lander site (**c, d**). Remotely operated underwater vehicle (ROV) image credits: ArcticNet/Canadian Scientific Submersible Facility (CSSF)/Department of Fisheries and Oceans (DFO). Laser points in panels **(c)** and **(d)** are 6 cm apart.

strate at the HSB lander location consisted mostly of pebbles, cobbles, and boulders (Fig. 2a, b; Kenchington et al., 2010; Dinn et al., 2020), whereas a visual assessment of the sediment type at the LSB lander location suggested the dominance of gravel (Cote, 2020). The seafloor at the HSB lander was characterized by large-sized massive demosponges (e.g. *Geodia* spp.), glass sponges (e.g. *Asconema* spp.), and large gorgonian corals (*Primnoa resedaeformis*; Fig. 2a, b; Kenchington et al., 2010; Dinn et al., 2020). The benthic community at LSB consisted mostly of small specimens of corals, including *Anthomastus* sp., and sponges such as *Polymastia* sp., *Craniella* sp., *Axinella* sp., and possibly *Mycale* sp. (Fig. 2c, d; Cote, 2020). The HSB lander was located on the shelf on a 2° slope, and the slope aspect was directed northwest at 60°. The LSB lander was located on the upper slope, east of the shelf break, on a 7° slope, and the slope aspect was directed southeast at 105° (Fig. S1 in the Supplement).

2.2 Sampling methodology

2.2.1 Near-bed lander deployment

Landers were deployed during research cruise *Amundsen* 2018 Leg 2C (27 July 2018) and retrieved during research cruise *Amundsen* 2019 Leg 1B (1 and 2 July 2019). The landers were each equipped with a 2 MHz single point measurement acoustic Doppler current profiler (ADCP; upward-looking, Nortek Aquadopp), a sediment trap, and a combined optical backscatter sensor (OBS) for turbidity and fluorescence (WET Labs ECO FLNTU).

The ADCPs collected data on pressure, water velocity, echo intensity (ABS; acoustic backscatter signal), and water temperature at a 10 min interval. Furthermore, the built-in accelerometer and magnetometer in the ADCPs collected data on heading, pitch, and roll. The ADCP was mounted 2 m above the bottom, and the blanking distance was 1.14 m. Velocity data were recorded in beam coordinates and transformed in MATLAB to ENU (east–north–up) coordinates after recovery using the transformation matrix provided by the manufacturer. The 2 MHz ADCPs have a lower particle size detection limit of 12 µm in diameter and a maximum sensitivity for particles of 242 µm diameter (Haalboom et al., 2021, 2023). The combined optical backscatter sensor for turbidity and fluorescence was programmed to measure every 10 min over the 1-year period. The sediment trap (PPS 4/3, Technicap Inc.), with a surface area of 0.05 m^2, was equipped with 12 bottles for suspended particulate matter collection and with the aperture mounted at 2 m above the bottom. Collection started on 15 August 2018 and lasted until the end of the deployment. Different time intervals of bottle rotation were set to increase the sampling resolution during the spring and summer months. The bottles rotated every 15 d from mid-August to mid-September 2018, every 30 d from mid-September to mid-November 2018, every 60 d from mid-November to mid-March 2019, every 30 d from mid-March to mid-May 2019, and every 15 d again from mid-May to mid-July 2019. Prior to deployment, a 4 % solution of formalin in brined seawater (40 psu, where psu denotes practical salinity units) was added to each bottle.

2.2.2 Water column and benthic sampling

CTD casts were performed over two cross-shelf transects crossing the LSB and HSB lander sites (Fig. 1b; Table S1;

Coté et al., 2018). Two CTD casts were carried out on the continental shelf and three on the continental slope, where the third or middle cast was performed above each benthic lander deployment. The CTD-rosette water column profiling and sampling package was equipped with a Sea-Bird SBE 911plus system, which contained sensors to measure temperature (Sea-Bird SBE 3plus), conductivity (Sea-Bird SBE 4), pressure (Paroscientific Digiquartz®), dissolved oxygen (Sea-Bird SBE 43), fluorescence (Seapoint), and a rosette water sampler with 12 Niskin bottles (12 L each). CTD data were processed and "cleaned" with the Sea-Bird SBE Data Processing software (Guillot, 2018). Water samples were taken from Niskin bottles at five depths (5 m, 50 m, mid-water, 100 m above bottom, and 10 m above bottom) for the determination of nutrients (NH_4^+, $NO_2^- + NO_3^-$, PO_4^{3-}, and SiO_2) and suspended particulate matter (SPM).

Benthic macrofauna samples for stable isotope analysis were collected at the two lander locations using a rock dredge on retrieval of the benthic landers (Table S2; Cote, 2020). A description of the species found at the two locations is given in Cote (2020). The rock dredge (7 mm mesh size) was deployed in "drift" mode at HSB, with a maximum speed of 2 kn ($\sim 4\,km\,h^{-1}$) for 10–20 min, and "tow" mode at LSB, with the ship moving at 1 kn for 10 min. During CCGS *Amundsen* cruise 2019 Leg 1B, it was the first time that a rock dredge had been operated on this research vessel; therefore, different operational modes of deployment were tested. At the LSB lander station, the rock dredge collected lots of soft sediment; therefore, drift mode was used. On deck, the dredge was rinsed, and the catch was subsampled and deposited in fish totes (64 L). The remaining material was sieved through a 2 mm mesh for the analysis of invertebrates and fishes. The total catch was photographed and preserved for species identification and quantification. Samples for stable isotopes were frozen (−20 °C) for further analysis at the Netherlands Institute for Sea Research (NIOZ).

2.2.3 Regional oceanography, sea-ice cover, and bottom temperature and salinity profiles

To explore the regional oceanography on the northern Labrador Shelf and upper slope, vertical Argo float profiles collected within the water depth range of 330–2575 m (Fig. S3) were extracted from the National Oceanic and Atmospheric Administration (NOAA) National Oceanographic Data Center (NODC) World Ocean Dataset and profiling Argo float Global Argo Data Repository archives (Kieke and Yashayaev, 2015; Yashayaev and Loder, 2017) using the approach of Kenchington et al. (2017). We used Argo float profile data ($N = 1472$) collected between 2005 and 2022 to determine the seasonal variability in temperature and salinity along the northwestern Labrador shelf break. Specifically, seawater properties of the corresponding water layers to the depth of the benthic landers (LSB = 350–450 m and HSB = 550–650 m depth) were assessed. We report the mean temperature and salinity values binned per water layer. Argo float profiles below ∼ 59° N latitude were considered LSB, whereas those above ∼ 59° N latitude were considered HSB. Temperature and salinity values were detrended for interannual variability using an eighth-degree least-squares polynomial fit. Time-averaged surface currents were derived from trajectories of satellite-tracked surface drifting buoys (drifters) deployed within the NOAA Global Drifter Program during 2000–2020 (Centurioni et al., 2019). The trajectories were obtained from delayed-mode hourly data and real-time variable time-step data (Elipot et al., 2016, 2022). The drifter data were temporally interpolated into 15 min time intervals, binned hourly, and a low-pass filter was used to remove tidal and inertial oscillations. Then, the surface velocities were binned into a 1/3° grid. The drifter-derived surface currents reveal well-defined large-scale cyclonic circulation of the Labrador Sea, recirculation gyres as well as mesoscale circulation features.

Sea-ice cover above the two benthic landers was extracted from weekly ice charts (Canadian Ice Service, 2022). Slope angle and aspect were estimated for each lander by taking the wider topography into account (Fig. S1; Gille et al., 2004). Along-slope and across-slope bottom velocities were derived from the bottom current direction, slope aspect, and bottom horizontal current speed.

2.3 Laboratory analysis

Water column nutrient concentrations were analysed with a SEAL QuAAtro analyser (Bran + Luebbe, Norderstedt, Germany) following standard colorimetric procedures. SPM samples were freeze-dried, weighed, and analysed for organic carbon content and total nitrogen content.

Sediment trap samples were filtered through a 1 mm sieve to remove large particles and swimmers, split into five subsamples using a McLane WSD-10 rotary splitter, rinsed with demineralized water to remove salts and formalin, and subsequently freeze-dried and weighed (Mienis et al., 2012; Newton et al., 1994). Lipids were extracted and analysed following the method of Kiriakoulakis et al. (2004). Briefly, samples were spiked with internal standard (5α(H)-cholestane), extracted by sonication in dichloromethane : methanol (9 : 1; $x3$). The solvent was removed, and samples were first trans-methylated (Christie, 1982) and then treated with bis-trimethylsilyltrifluoroacetimide: trimethylsilane (99 : 1; 30–50 µL; 60 °C; 1 h) prior to analysis by gas chromatography–mass spectrometry (GC–MS). GC–MS analyses were conducted using a GC TRACE 1300 fitted with a split/splitless injector and DB-5MS column (60 m × 0.25 mm internal diameter, a film thickness of 0.1 µm, and a non-polar stationary phase of 5 % phenyl and 95 % methyl silicone), using helium as a carrier gas ($2\,mL\,min^{-1}$). The GC oven was programmed to rise from 60 to 170 °C at $6\,°C\,min^{-1}$ after 1 min, then from 170 to 315 °C at $2.5\,°C\,min^{-1}$, and was finally held at 315 °C for 15 min. The eluent from the GC was transferred directly

via a transfer line (320 °C) to the electron impact source of a Thermoquest ISQMS single quadrupole mass spectrometer. Typical operating conditions were as follows: ionization potential of 70 eV, source temperature of 215 °, and trap current of 300 µA. Mass data were collected at a resolution of 600 Da, cycling every second from 50 to 600 Da and were processed using Xcalibur software.

Compounds were identified by comparison of their mass spectra and relative retention indices with those available in the literature or by comparison with authentic standards. Quantitative data were calculated by comparison of peak areas of the internal standard with those of the compounds of interest, using the total ion current (TIC) chromatogram. The relative response factors of the analytes were determined individually for 36 representative fatty acids and sterols using authentic standards. Response factors for analytes where standards were unavailable were assumed to be identical to those of available compounds of the same class.

Sponges and other benthic fauna collected using a rock dredge were subsampled aboard the CCGS *Amundsen*, as some parts of the specimens' bodies were used in separate studies and other parts for isotopic analysis in this study. In the laboratory, the collected fauna was freeze-dried and homogenized with a pestle mortar and ball mill. Subsamples (ca. 10 mg) were transferred into silver cups and acidified by addition of dilute HCL (2 %, 5 %, and 30 %) to remove carbonates. Organic carbon and $\delta^{13}C$ were analysed on acidified subsamples, and total nitrogen and $\delta^{15}N$ was determined on non-acidified subsamples using an electron analyser coupled to an isotope ratio mass spectrometer (Thermo FlashEA 1112). The $\delta^{13}C$ and $\delta^{15}N$ isotope values are expressed in parts per thousand (‰) relative to the international standard Vienna Pee Dee Belemnite and atmospheric N_2 for carbon and nitrogen, respectively. The standard deviation of $\delta^{13}C$ and $\delta^{15}N$ measurements was 0.15 ‰.

2.4 Data analysis

2.4.1 Data processing

The transformation of beam coordinates to ENU coordinates for the ADCP data was carried out in MATLAB (MATLAB, 2010), and other data processing steps used R. The following R packages are used during data analysis: oce, ggplot2, RColorBrewer, knitr, reshape2, RNetCDF, readxl, lubridate, xts, tibble, dplyr, mapdata, patchwork, tibbletime, readr, signal, astsa, and terra (Hijmans, 2023; Becker et al., 2022; Campitelli, 2021; Grolemund and Wickham, 2011; Kelley and Richards, 2020; Michna and Woods, 2019; Müller and Wickham, 2023; Neuwirth, 2022; Pedersen, 2019; R Core Team, 2019; Ryan and Ulrich, 2023; signal developers, 2023; Stoffer, 2020; Vaughan and Dancho, 2020; Wickham, 2007, 2016; Wickham and Bryan, 2019; Xie, 2020). Statistics are presented as means ± standard deviations.

2.4.2 Benthic lander analysis

Occasionally, pitch and roll data from the ADCP sensor at HSB were shifted for a small period of the deployment, implying that the lander was occasionally moving slightly (Fig. S3). The pitch, heading, and roll were almost identical before and after these disturbances. Furthermore, the ADCPs correct for the pitch, heading, and roll of the respective device when producing the raw beam data. Removing data points during disturbance did not change the outcome of any of the analyses, statistical tests, or descriptive statistics; therefore, data points were retained in the HSB lander time series.

Chl-*a* concentration (in $\mu g\,L^{-1}$) and turbidity (in nephelometric turbidity units, NTUs) were calculated from ping counts as described in the manual of the manufacturer.

Spectral analyses of lander data based on a Fourier transformation (Bloomfield, 2004) were performed to examine recurring patterns or periodicity in the time-series data (e.g. Shumway et al., 2000; Bloomfield, 2004). Prior to these analyses, time-series data were smoothed using modified low-pass Daniell filters (Bloomfield, 2004), to remove periodicities shorter than 3 h. The magnitude and direction of ADCP-recorded tidal currents were analysed with least-squares harmonic analysis.

2.4.3 Critical slope and comparing barotropic with baroclinic tides

Internal tides are generated by the barotropic tide interacting with sloping bottom topography and can have a profound influence on the thermohaline structure and local mixing processes. Internal tides are found at complex deep-sea topographic features such as continental shelves, ridges, seamounts, and canyons (e.g. Cacchione et al., 2002). Internal tide–topography interactions can be classified by the slope parameter α/c (St Laurent et al., 2003; Cacchione et al., 2002). The internal wave slope c is calculated with Eq. (1):

$$c = \sqrt{\frac{\omega^2 - f^2}{N^2 - \omega^2}} \tag{1}$$

with tidal frequency $\omega = 1.4053 \times 10^{-4}\,\mathrm{rad\,s^{-1}}$ (representing the dominant M2 tidal component) and local inertial frequency f (s^{-1}). The Brunt–Väisälä frequency N^2 ($\mathrm{rad\,s^{-2}}$) was calculated as the mean value ($1.4228 \times 10^{-5}\,\mathrm{rad\,s^{-2}}$) from all CTD stations and depths below the deep pycnocline at 250 m or from bottom values at shallower profiles. The topographic slope α was calculated from the maximum depth gradients in latitude and longitude based on GEBCO_2023 data (GEBCO Bathymetric Compilation Group, 2023). At critical or near-critical slopes ($\alpha \approx c$), the internal tide is locally amplified and vertical mixing is intensified. At sub-critical slopes ($\alpha < c$), internal waves pass the

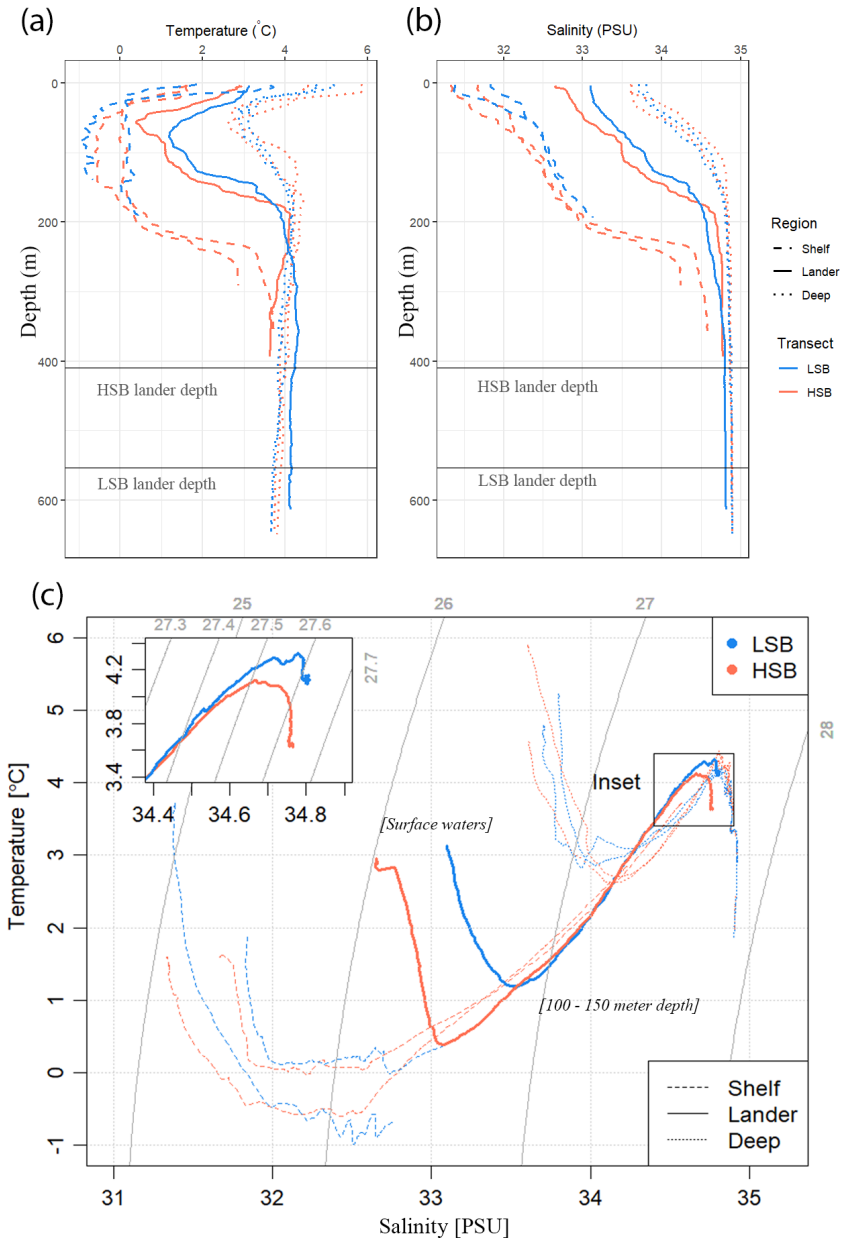

Figure 3. Hydrographic conditions in the study area: **(a)** temperature, **(b)** salinity, and **(c)** temperature–salinity (TS) plots for the two transects. LSB denotes the low-sponge-biomass transect, whereas HSB denotes the high-sponge-biomass transect. Depths of landers are indicated by the horizontal grey lines in panels **(a)** and **(b)**. The temperature and salinity profiles in panels **(a)** and **(b)** only show the top 600 m, whereas TS plots in panel **(c)** include the entire water column. The thin grey lines in panel **(c)** resemble isopycnals.

topographic slope without being locally modified. At steeper super-critical slopes ($\alpha > c$), internal waves are reflected into deeper waters. Bottom currents and direction were compared to model-derived barotropic tidal currents, retrieved from the Oregon State University (OSU) Tidal Inversion Software (OTIS; Egbert and Erofeeva, 2002).

3 Results

3.1 Seawater properties over the northern Labrador Shelf and upper slope

The CTD casts, performed in July 2018, revealed different seawater properties between the two transects (Figs. 3, S4). The surface water at the time of survey was relatively warm (2–6 °C) and fresh (31.2 to 33.8 psu) with an offshore increase in temperature and salinity. From the surface to a

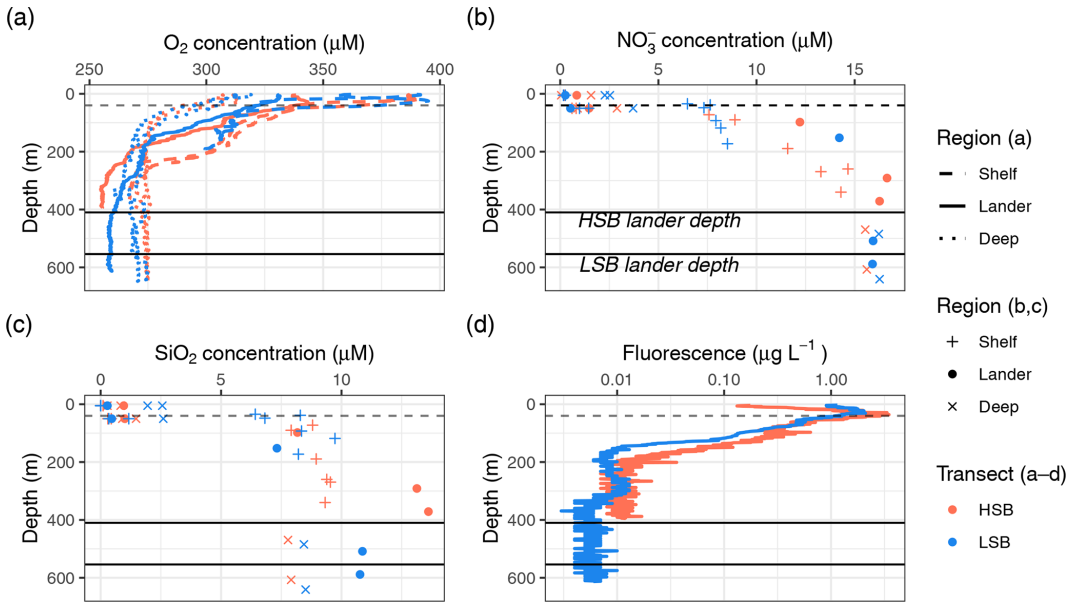

Figure 4. The **(a)** oxygen, **(b)** nitrate, and **(c)** silicate concentration profiles for the two transects and **(d)** fluorescence profiles for the two CTD casts above the two lander locations. HSB denotes the high-sponge-biomass site, whereas LSB denotes the low-sponge-biomass site. Black lines indicate lander depths, whereas dashed lines indicate the thermocline.

depth of 20–70 m, depending on the transect and location, temperature decreased to sub-zero or near-zero at the shelf locations and to 3 °C at the slope locations; it then increased again to 2.8 °C at 250 m depth on the shelf and to 4.3 °C at 150 m on the slope. A cold intermediate layer was visible at all profiles between 50 and 150 m depth. Salinity increased nearly monotonically with depth up to the pycnocline across all stations. The stations at LSB were more saline overall than those at matching water depths on the HSB transect. Buoyancy frequency showed peak values at the upper and lower boundaries of the above-described cold intermediate layer at both transects (Fig. S4f).

The oxygen concentration was highest in the surface waters (0–50 m) on the shelf and decreased with depth at all CTD stations (Fig. 4a). Although oxygen concentrations were still generally high, the bottom oxygen concentrations at the lander stations were, for both transects, relatively depleted compared with the deep-water CTD transects at similar depths. Concentrations of nitrate, phosphate, and silicate were lowest above the thermocline and increased with depth, while ammonium and nitrite were higher near the surface than at depth (Figs. 4b and c, S5). The HSB station exhibited relatively high nitrate, phosphate, and silicate concentrations at 10 and 100 m above bottom compared with similar depths at shelf and deep stations (Figs. 4b and c, S5). This increased nutrient concentration in the bottom waters was also apparent for silicate at the LSB station (Fig. 4c), although not for nitrate (Fig. 4b). Chl-*a* profiles showed a deep chlorophyll maximum along both transects at 50 m (Fig. 4c) as well as near-zero concentrations in the bottom waters (Fig. S4d). Particulate organic carbon (POC) concentrations were highest in the surface waters (8–38 µmol POC L^{-1}) and on the shelf (Fig. S6). POC concentrations decreased with depth, and concentrations 10 m above bottom were 1.48 µmol POC L^{-1} at HSB and 5.95 µmol POC L^{-1} at LSB.

Surface water above the benthic lander locations was partly ice-covered from December to June, but both sites were located at the sea-ice border in the study area and ice cover was highly variable (Fig. S11). Only during January was ice coverage above 70 % at both sites. Both locations showed a short ice-free period in February and March. During the spring bloom, between the end of March and early May, sea-ice coverage tended to be higher at HSB than at LSB (Fig. S11d).

3.2 Regional oceanography and seasonal temperature patterns

Surface buoy drifter data showed that the HSB lander was located in an area where three (surface) currents converge (Fig. 5a). Strong surface currents (> 0.24 m s^{-1} on average) carry water from the Hudson Strait towards the Labrador shelf break, where this current meets two others that flowed toward the HSB site from the north and northeast, respectively. On convergence, the currents followed the bathymetry of the Labrador shelf break or upper slope in a southward direction.

The seawater in the region of HSB was warmer and less saline than around LSB for both depth ranges within which the landers were deployed (Figs. 5b and c, S7). Bottom-water temperature shows a steeper decrease in February at LSB

compared with HSB (Fig. 5c). Temperature and salinity show higher scatter at HSB than LSB throughout the season, but variability in temperature is highest at HSB in February and March (Figs. 5b and c, S7).

3.3 Year-long near-bottom measurements

3.3.1 Near-bottom current velocities

In general, bottom current speeds were higher at the HSB compared with the LSB station (Table 1; Fig. 7). General current direction was southeasterly at HSB and south-southwesterly at LSB (Fig. 6). Vertical velocity (w) was on average upward and comparable between HSB and LSB, but the range in vertical velocity was higher at HSB (-0.35 to $0.32\,m\,s^{-1}$) compared with LSB (-0.11 to $0.21\,m\,s^{-1}$; Fig. 7c). Bottom horizontal currents were twice as high at HSB compared with LSB (Table 1), and peak bottom horizontal current speeds were $0.75\,m\,s^{-1}$ (HSB) and $0.65\,m\,s^{-1}$ (LSB), with the third quantile at $0.33\,m\,s^{-1}$ (HSB) and $0.18\,m\,s^{-1}$ (LSB).

3.3.2 Near-bottom environmental conditions

Bottom temperature was slightly warmer at HSB compared with LSB and increased at both sites (0.2–0.3 °C) during December and January (Fig. 9). The benthic lander temperature aligned well with the seasonal temperature pattern retrieved by Argo float profiles (Fig. 5b, c). Turbidity measured by ABS was similar for the two stations (Table 1; Fig. 9b) and showed higher values in winter months. Chl-*a* remained low from October to February–March, after which time values started to increase for both landers (Fig. 9c). Bottom Chl-*a* concentrations started to increase after short ice-free periods in mid-February and mid-March (Figs. 9c, S11d). The HSB station showed highest Chl-*a* concentrations from mid-March to the end of May, while increased concentrations were observed at the LSB station from mid-March to early May.

Turbidity measured by OBS was elevated at HSB from February to April and at LSB from December to January. The higher variability in Chl-*a* and turbidity at the LSB site over the year (Table 1) was caused by several peaks in Chl-*a* and turbidity that were an order of magnitude higher than average values (Fig. S8).

During several periods in the year-long time series, turbidity measured by the ABS increased at the turning of the tide and at high southeasterly current velocities at HSB (see e.g. Fig. 10b and g). Strong along-slope (southerly) bottom currents increased ABS turbidity at LSB (Fig. 10a and g). Across- and along-slope water transport influenced bottom temperature. At the HSB lander, for example, in the first week of September, temperature decreased when the current was directed northwest and increased when the current was directed southeast (Figs. 10a and f, S9).

Table 1. Benthic lander values over the year-long deployment period. Values are given as the mean ± standard deviation. HSB denotes the high-sponge-biomass lander, LSB denotes the low-sponge-biomass lander, ABS represents the acoustic backscatter signal, and OBS represents the optical backscatter signal.

Variable	HSB	LSB
u (eastward velocity; $m\,s^{-1}$)	0.05 ± 0.22	-0.01 ± 0.09
v (northward velocity; $m\,s^{-1}$)	-0.07 ± 0.16	-0.09 ± 0.11
w (vertical velocity; $m\,s^{-1}$)	0.03 ± 0.05	0.02 ± 0.03
Bottom current speed ($m\,s^{-1}$)	0.26 ± 0.14	0.14 ± 0.08
Temperature (°C)	3.70 ± 0.17	3.58 ± 0.17
Daily temperature variability ($\Delta\,°C\,d^{-1}$)	0.25 ± 0.16	0.17 ± 0.1
Turbidity by ABS (counts)	98.1 ± 9.8	96.6 ± 11.0
Chl-*a* concentration ($\mu g\,L^{-1}$)	0.11 ± 0.03	0.08 ± 0.10
Turbidity by OBS (NTU)	0.20 ± 0.10	0.21 ± 0.27
Across-slope velocity ($m\,s^{-1}$)	0.01 ± 0.13	-0.01 ± 0.01
Along-slope velocity ($m\,s^{-1}$)	-0.08 ± 0.23	-0.09 ± 0.11

3.3.3 Tidal analysis of bottom currents and environmental conditions

Bottom current speeds showed semidiurnal and spring–neap tidal patterns, with a peak every fortnight for both sites (Figs. 7, 8b, 10). The major axes of the semidiurnal tidal ellipses were orientated in a northwest–southeast direction at HSB and a north–south direction at LSB (Fig. 8a, b). The tidal analysis presented in Table 2 and Fig. 8 shows notable differences in tidal characteristics between the LSB and HSB lander locations. While semidiurnal tidal harmonics predominate at both locations, the semi-major axis at the HSB site is approximately 4 times larger than the corresponding value at the LSB site. Moreover, there is a significant discrepancy between the modelled and observed main semidiurnal tidal harmonics (M2) at the HSB site, particularly in terms of magnitude and tidal ellipse eccentricity. This indicates that the dominant barotropic semidiurnal tide (M2) is altered at the HSB site, leading to strongly rectified near-bottom baroclinic tidal currents. There are no substantial differences between the modelled (barotropic) and observed S2 tidal currents, except for the tidal ellipse eccentricity at the LSB site, likely due to the depth difference between the model and observations at this location. Furthermore, spectral density for the HSB bottom current components also peaked at shorter frequencies (3–6 h) and at the 14 d spring–neap tide (Fig. 8c). In addition, a superimposed seasonal pattern can be seen at both sites, where the bottom current speed gradually increased from July 2018 to March 2019 and decreased again from March to July 2019 (Fig. 7d).

Temperature, Chl-*a*, and turbidity measured by ABS and OBS all showed a reoccurring tidal peak, with higher peaks in spectral density for the semidiurnal periodicity at HSB than at LSB (Fig. 8d). Daily temperature fluctuations were

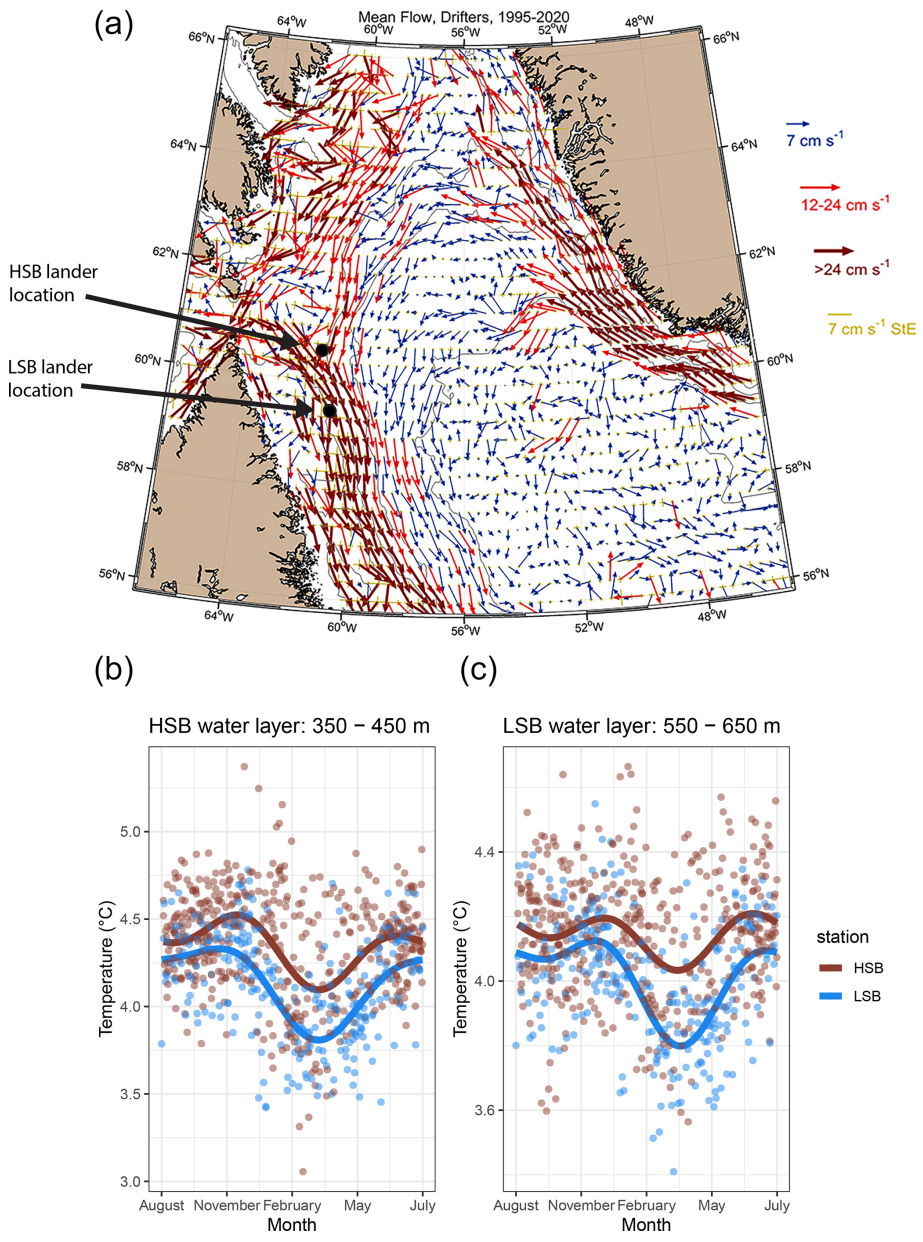

Figure 5. (a) The general surface circulation pattern in the Labrador Sea based on drifter buoy data spanning from 1995 to 2020. Arrows indicate the mean direction; the colours and lengths of arrows present the strength of the mean flow, and the yellow arrows present the standard error of the flow over the 1995–2020 period. The lander locations are indicated by the coloured dots. **(b, c)** Seasonal temperature, from Argo float profiles, of the water layer in which the HSB or LSB lander was located. Dots represent individual water-layer-binned temperature measurements vs. day of the year. The lines are a smoothed fit that show the seasonal pattern.

higher at HSB than at LSB. During the spring bloom, the bottom Chl-*a* concentration increased during strong south-easterly current velocities at HSB (Fig. S10) and showed a periodic reoccurring peak (Fig. S11a).

3.4 Mass deposition and organic carbon fluxes

The average mass fluxes were higher at HSB ($2.46 \pm 1.76\,\mathrm{g\,m^{-2}\,d^{-1}}$) than at LSB ($1.43 \pm 0.93\,\mathrm{g\,m^{-2}\,d^{-1}}$), with highest fluxes in winter (October–April) at both sites, which corresponds well with the superimposed seasonal patterns seen in ABS turbidity and bottom current speed. Average POC fluxes were higher at HSB ($3.07 \pm 1.91\,\mathrm{mmol\,C\,m^{-2}\,d^{-1}}$) than at LSB ($1.91 \pm 0.71\,\mathrm{mmol\,C\,m^{-2}\,d^{-1}}$). Organic carbon content at HSB was highest in autumn and summer months ($\sim 2\,\%$) and highest at LSB in autumn (2 %–4 %; data not shown). Average C : N ratios were lower at HSB (8.6 ± 3.2) than at LSB (10.8 ± 2.7)

Table 2. Tidal analysis of velocity time series from the HSB and LSB lander sites based on ADCP measurements and OTIS tidal model analysis. The terms a_{maj} and a_{min} represent the respective semi-major and semi-minor axes of the tidal ellipse and ε is the eccentricity (a_{min}/a_{maj}). OTIS model data represent the barotropic tidal signal, whereas ADCP data show the near-bottom tidal characteristics.

LSB lander data	a_{maj} (cm s^{-1})	a_{min} (cm s^{-1})	ε (a_{min}/a_{maj})	Water depth (m)
M2	5.73	2.17	0.38	558
S2	1.74	0.51	0.30	
K1	0.65	0.05	0.08	
O1	0.10	0.03	0.25	
HSB lander data				
M2	27.77	7.26	0.26	410
S2	9.61	2.88	0.30	
K1	0.88	0.44	0.51	
O1	0.36	0.21	0.58	
LSB OTIS tidal model				
M2	6.08	1.48	0.24	629
S2	1.58	0.57	0.36	
K1	0.49	0.06	0.11	
O1	0.18	0.01	0.04	
HSB OTIS tidal model				
M2	40.67	19.23	0.47	425
S2	10.45	4.47	0.43	
K1	1.35	0.53	0.39	
O1	0.80	0.38	0.48	

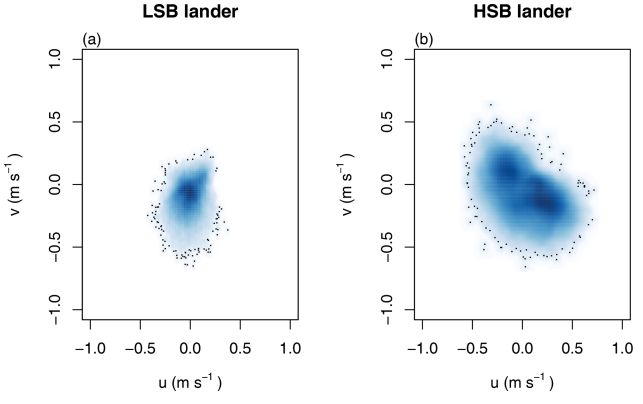

Figure 6. Horizontal current velocities at the **(a)** LSB lander and **(b)** HSB lander.

and were higher in winter and also in May 2018 (Fig. 11c). The δ^{13}C ratios of trapped material were higher in winter at HSB compared with LSB and were higher in summer at LSB than at HSB (Fig. 11d). The δ^{15}N of trapped material was comparable between sites, although slightly higher at LSB. Winter δ^{15}N values were highest compared with the rest of the year for both landers (Fig. 11e). The lipid flux was slightly higher at LSB, with low values in winter and peak values during the spring bloom (Fig. 11f). Unsaturated alcohols comprised the largest fraction of lipids at LSB, especially in autumn and winter (Fig. S12b). Peak lipid flux in April consisted of 25 % polyunsaturated fatty acids (PUFAs) at HSB (Fig. S12c). Sterols made up the largest fraction of total lipids at HSB and LSB in May (Fig. S12d). The sterol fraction was lower in spring at both sites. Swimmers were found in the sediment trap bottles, especially in the autumn months at LSB. These consisted mostly of copepods (e.g. *Calanus* sp.), mysids (e.g. *Boreomysis* sp.), amphipods (e.g. Eusiridae), and chaetognaths (i.e. arrow worms). Numbers of trapped swimmers were lowest during winter at both sites. In addition, several large sponge spicules were found in the bottles at HSB but not at LSB.

3.5 The δ^{13}C and δ^{15}N isotopic ratios of benthic fauna and trapped material

The massive sponge *Geodia* spp. sampled at HSB showed a distinct isotopic signature compared with the other benthic organisms, with a relatively enriched δ^{13}C value (-18.55 ± 0.17 ‰) and a low δ^{15}N value (8.24 ± 0.16 ‰; Fig. 12). The gorgonian coral *Primnoa resedaeformis* had a δ^{13}C value of -21.19 ± 0.59 ‰ and a δ^{15}N value of 10.54 ± 0.33 ‰. Compared with *P. resedaeformis*, Decapoda sp. showed slightly enriched δ^{13}C (-20.48 ± 0.31 ‰) and δ^{15}N (11.97 ± 0.43 ‰) values. The glass sponge *Asconema* sp., sampled at HSB, also had relatively enriched isotopic values (δ^{13}C: -20.27 ± 0.36 ‰; δ^{15}N: 12.57 ± 0.31 ‰), while the sponge *Mycale*

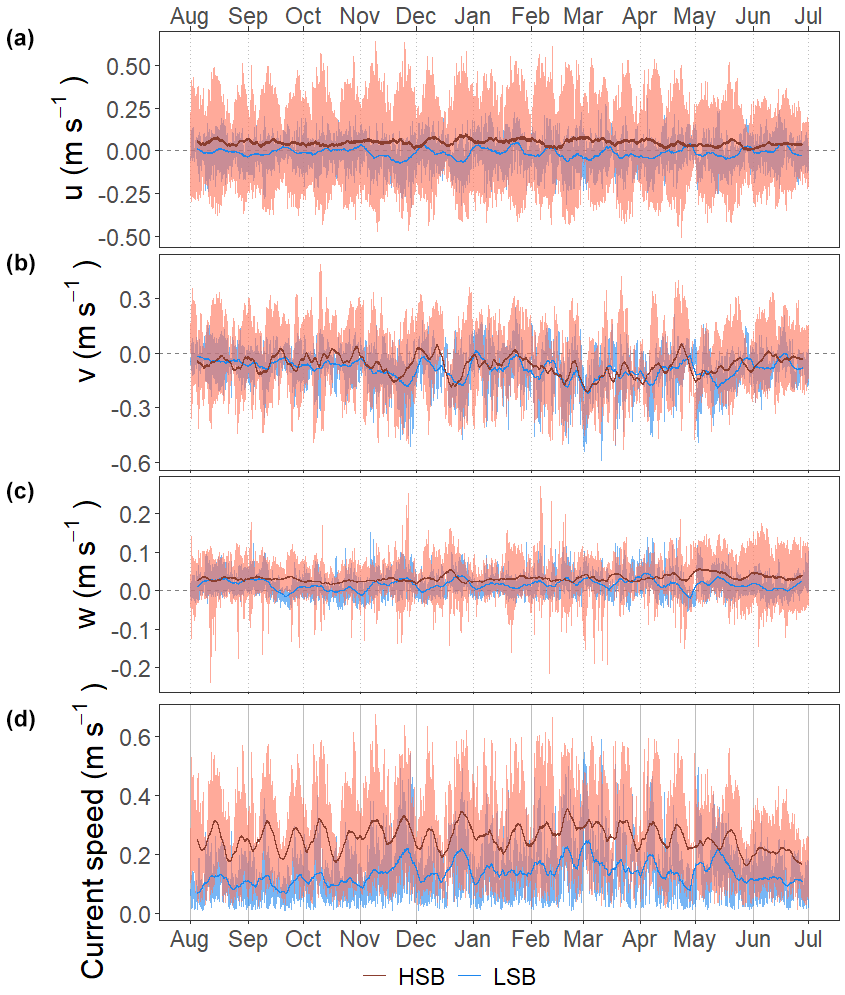

Figure 7. Time series of the flow velocities with eastward u velocity **(a)**, northward v velocity **(b)**, and vertical w velocity **(c)** and of the bottom current speed **(d)**. Plots show the hourly averaged data as transparent lines and the 7 d rolling means as solid lines.

sp., sampled at LSB, had a high δ^{15}N isotopic ratio (13.05 ± 0.41 ‰) and a δ^{13}C ratio of −19.47 ± 0.06 ‰. Sediment trap samples had the lowest δ^{15}N and δ^{13}C isotopic ratios, with only small differences between HSB and LSB (Figs. 11d and e, 12).

4 Discussion

Hydrodynamic and environmental conditions were compared at two contrasting high- and low-sponge-biomass sites along the northern Labrador shelf break. The aim was to compare differences between the two sites in terms of (i) seawater properties and regional hydrography (Sect. 4.1 and 4.2); (ii) bottom currents and environmental conditions, including seasonal variations over the course of a year (Sect. 4.3 and 4.4); and (iii) benthic–pelagic coupling, organic matter supply, and isotopic signatures of benthic macrofauna (Sect. 4.6, 4.6, and 4.7).

4.1 Regional oceanography on the northern Labrador Shelf and Labrador Slope

The northern Labrador Shelf and Labrador Slope are known to be subject to strong tidal forcing which causes vertical mixing, high bottom current speeds (Drinkwater and Jones, 1987; Griffiths et al., 1981), and reduced stratification compared with the more northerly Baffin Island shelf (Lazier, 1982; Sutcliffe et al., 1983; Drinkwater and Harding, 2001). The results of our drifter analysis confirm that three currents converge around the HSB area: the Hudson Strait outflow water, the Baffin Intermediate Current, and the West Greenland Current (Fig. 5a; Ricketts et al., 1931; Yashayaev, 2007; Straneo and Saucier, 2008; Curry et al., 2011, 2014). These three respective currents transport Hudson Strait outflow water, Arctic Water and/or Baffin Bay (intermediate) Water, and Irminger Water towards the northern Labrador Shelf and upper slope. Our CTD transects show that the characteristics of these water masses and are similar to earlier observations

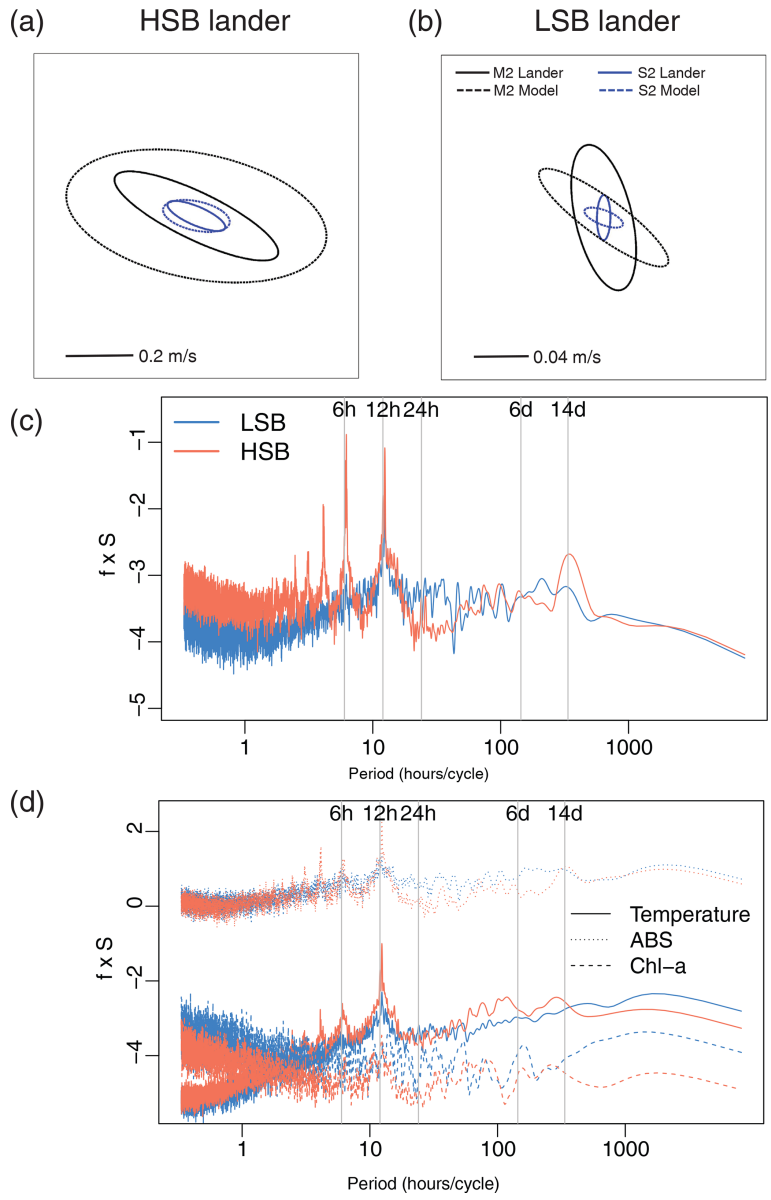

Figure 8. (a, b) Tidal current ellipses at the HSB and LSB lander sites for the two dominant semidiurnal tidal harmonics M2 (black lines) and S2 (blue lines) derived from the unfiltered ADCP velocities (solid lines) and the OTIS inverse tidal model (dashed lines), respectively. Variance-preserving spectra for **(c)** bottom current speed, **(d)** temperature, turbidity by acoustic backscatter signal (ABS), and Chl-*a*.

(Drinkwater and Harding, 2001; Fissel and Lemon, 1991; Petrie et al., 1988). The warmer and saltier water at HSB (temperature $\sim 4.5\,^{\circ}C$ and salinity ~ 34.9) compared with LSB is likely caused by Irminger Water (Fig. 5b, c), which follows the Labrador Slope in a cyclonic direction beneath the cold water of the West Greenland Current and above the upper slope (Lazier et al., 2002). Our findings concur with previous work which showed that Irminger Water is gradually cooled while moving southward by mixing with the Baffin Island Current (Cuny et al., 2002). However, the Argo float temperature profiles indicate that the area around HSB might play an important role in transforming Irminger Water. For example, the 350–450 m depth layer in the HSB area regularly showed the presence of Irminger Water ($> 4.5\,^{\circ}C$), while it was only sporadically measured at LSB (Fig. 5b). Irminger Water might, therefore, be cooled and freshened in the area around HSB due to convergence and, consequently, mixing occurs with the Hudson Outflow and Baffin Island Current. Our results support earlier findings that identified a connection between the Hudson Strait outflow strength and the southern Labrador Shelf water based on salinity measurements (Myers et al., 1990; Sutcliffe et al., 1983).

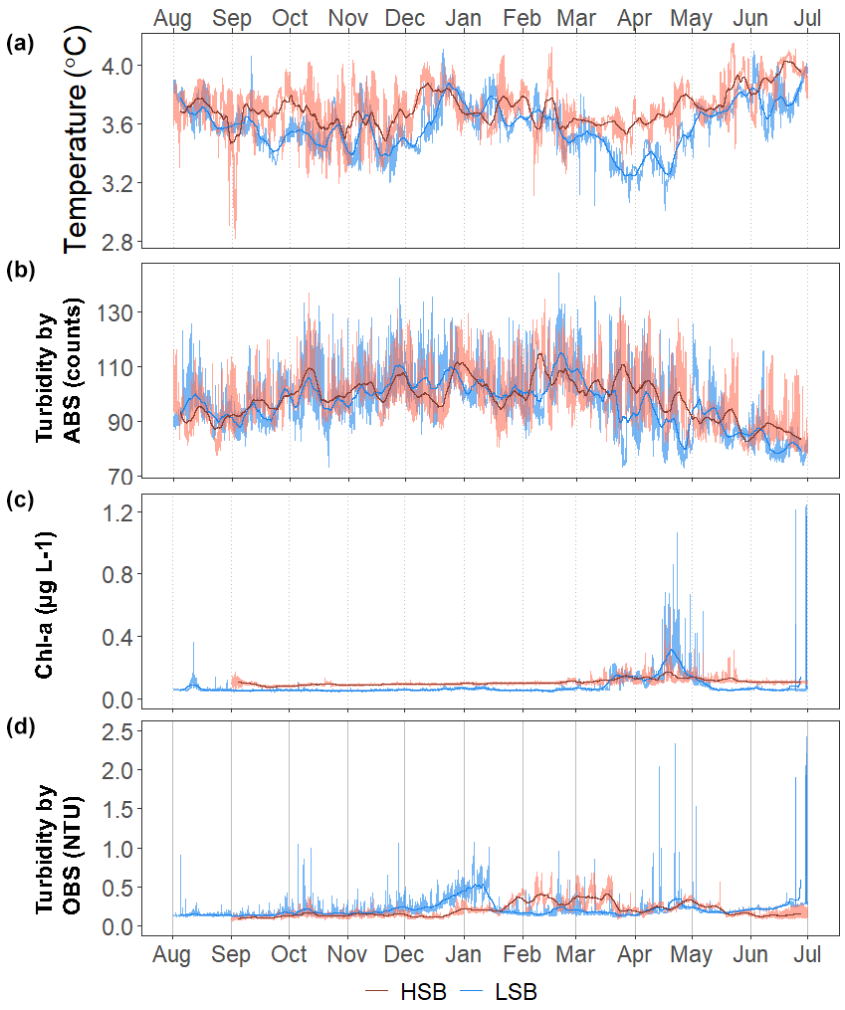

Figure 9. Time series for **(a)** temperature (in °C), **(b)** turbidity by acoustic backscatter (ABS; in counts), **(c)** Chl-*a* concentration (in µg L^{-1}), and **(d)** turbidity by optical backscatter (OBS; in NTU). For clarity, panels **(c)** and **(d)** are limited to 1.25 µg L^{-1} and 2.5 NTU on the *y* axis, respectively. Chl-*a* and turbidity from OBS data without the *y*-axis cut-offs are plotted in Fig. S10.

4.2 Increased bottom nutrient concentrations

Both the LSB and HSB lander sites showed higher nutrient concentrations in the bottom water compared with the other shelf and deep CTD stations, and this difference was more pronounced at the HSB lander location (Fig. 4). Here, we discuss two possible explanations for this observation: large-scale advection of nutrient-rich water from Baffin Bay and sediment efflux of silicic acid. Firstly, nutrient-rich intermediate water flows from Baffin Bay via the Davis Strait southward along the continental slope (Curry et al., 2014). This water mass, referred to as Baffin Bay Water (BBW), contains high nutrient concentrations (e.g. 41.6 ± 25.5 µM $Si(OH)_4$, 18.5 ± 2.6 µM NO_3^-; Sherwood et al., 2021) due to in situ remineralization of organic matter to deep water circulating in the Baffin Bay basin (Jones et al., 1984; Lehmann et al., 2019; Tremblay et al., 2002). Furthermore, BBW shows relatively high concentrations of silicate and phosphate compared with nitrate, due to denitrification at depth in Baffin Bay (Lehmann et al., 2019; Sherwood et al., 2021). This water mass could have enhanced local bottom-water nutrient concentrations at the HSB sponge ground. Secondly, high efflux of silicic acid (nutrients) from the sediment could enhance bottom-water silicate (nutrient) concentrations. Research on glass-sponge grounds on the Scotian Shelf has shown that biogenic silica efflux from sediments leads to higher bottom silicate concentrations (Maldonado et al., 2020b). This would also be possible for our study area. Given that the silicate concentration was elevated by ∼ 2–3 µM up to 100 m above the bottom (Fig. 4), assuming that the length of the sponge ground was ∼ 120 km (Fig. 1), and thereby estimating that the retention time of a water parcel on the sponge grounds is about 33 d (the length of sponge ground divided by residual current speed), this would mean that, under the assumption that the bottom 100 m is well mixed, a sediment efflux of 6–9 mmol Si m^{-2} d^{-1}

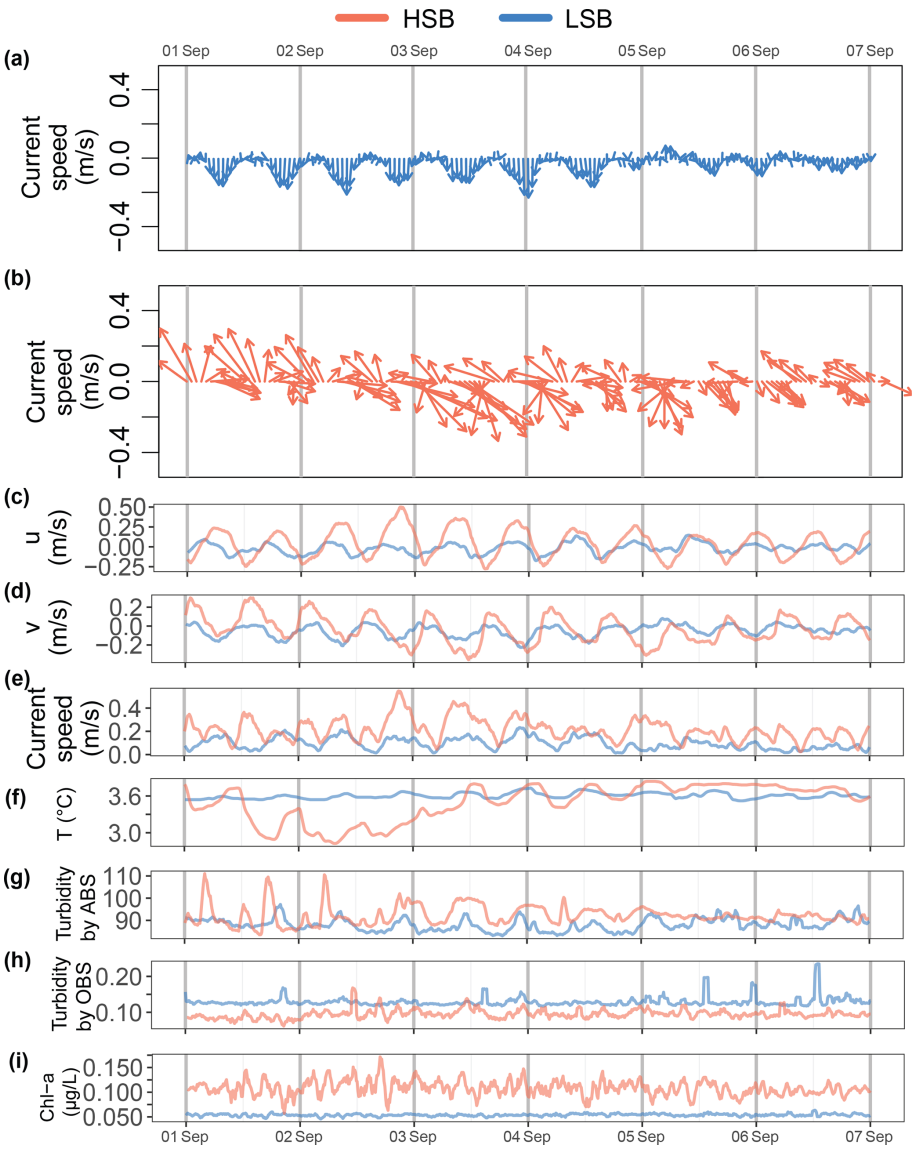

Figure 10. Expanded detail for the first week of September for the **(a)** current direction at LSB, **(b)** current direction at HSB, **(c)** eastward velocity, **(d)** northward velocity v, **(e)** bottom current speed, **(f)** temperature, **(g)** turbidity by acoustic backscatter (ABS), **(h)** turbidity, and **(i)** Chl-*a* concentration.

would be required. While this would be a substantial sediment efflux, silicate effluxes of 2.4 mmol Si m^{-2} d^{-1} have been measured on the Scotian Shelf (Andrews and Hargrave, 1984; Maldonado et al., 2020b), and values of up to 14.1 mmol Si m^{-2} d^{-1} have been observed in the Laurentian Channel (Eastern Canada; similar depth and temperature; Miatta and Snelgrove, 2021). Nonetheless, the higher silicate concentrations at the HSB lander compared with those at the LSB lander imply that the source is located closer to HSB. The fact that phosphate was also enhanced in bottom waters at HSB suggests that the advection of nutrient-rich water from upstream is the more probable explanation. However, further work on bottom silicate concentrations in relation to sponge grounds in this area is needed to unravel the source of this excess silicate and investigate if and how sponge grounds benefit from this.

The elevated nutrient concentrations could be beneficial for benthic organisms, specifically deep-sea sponges, which require silicic acid for spicule formation and skeletal growth (López-Acosta et al., 2016; Maldonado et al., 2011, 2020a; Whitney et al., 2005). Published kinetic uptake curves, describing the silicic acid uptake rate vs. concentration, suggest that the higher concentration at the HSB lander (13.6 µM) compared with LSB shelf (9.3 µM) led to a higher silicic acid uptake rate at the HSB site of 39 % for *Axinella* spp. and 40 % for *V. pourtalesii* (Maldonado et al., 2011, 2020a).

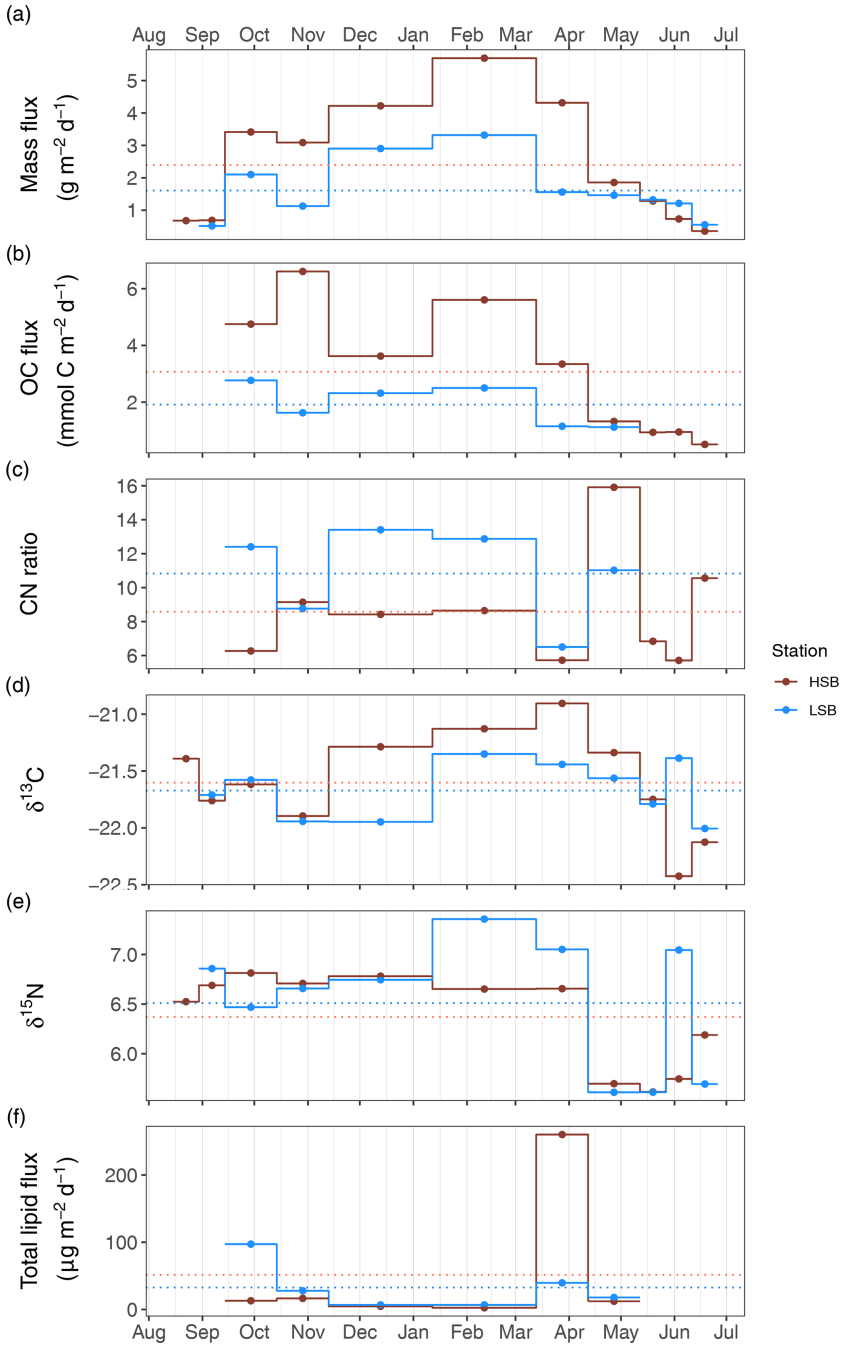

Figure 11. Sediment trap content from the two benthic landers. HSB denotes the high-sponge-biomass lander, whereas LSB denotes the low-sponge-biomass lander. Panel **(a)** shows the mass flux (in g $m^{-2}d^{-1}$), panel **(b)** shows the organic carbon flux (in mmol C m^{-2} d^{-1}), panel **(c)** presents the molar C : N ratio of trapped material, panel **(d)** presents the $\delta^{13}C$ of trapped material, panel **(e)** shows the $\delta^{15}N$ of trapped material, and panel **(f)** shows the total lipid flux (in µg m^{-2} d^{-1}).

Furthermore, elevated silicic acid concentrations on a spatial scale of kilometres are thought to allow the persistence of sponge grounds and the build-up of (glass-) sponge biomass over long timescales (Maldonado et al., 2020b; Whitney et al., 2005).

4.3 Tidal dynamics and bottom current speed

This study is, to our knowledge, the first to report year-long hydrodynamic and environmental conditions measured simultaneously at a high- and low-sponge-biomass ground. Our measurements show high bottom currents at both sites

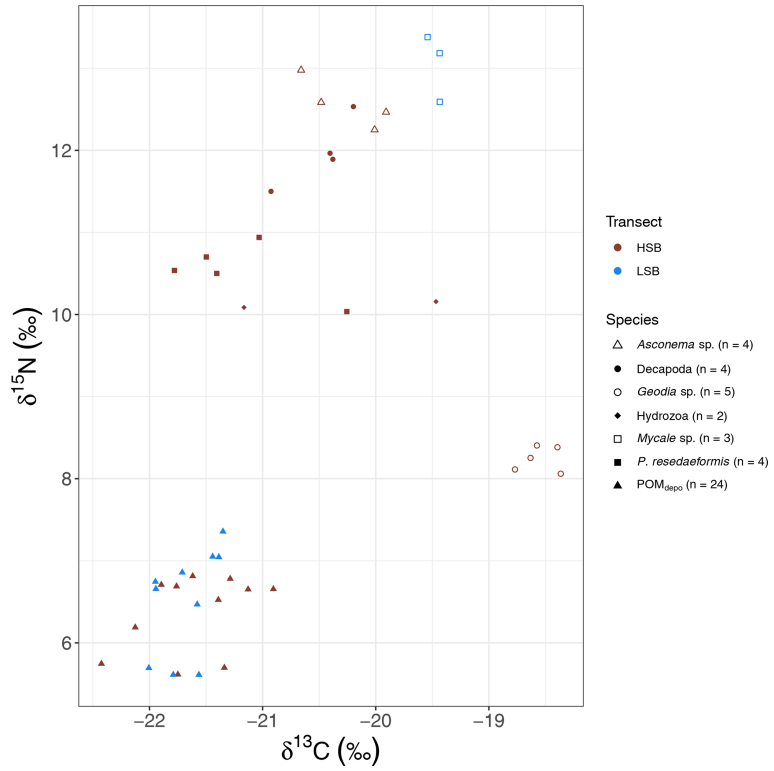

Figure 12. Carbon and nitrogen stable isotope plots of megafauna and sediment trap samples. HSB denotes high-sponge-biomass sites, whereas LSB denotes low-sponge-biomass sites.

with distinct differences in tidal dynamics. While semidiurnal tidal harmonics predominate at both sites, tidally driven horizontal current speeds were around 4 times higher at HSB than at LSB. At the HSB site, barotropic and near-bottom M2 tidal currents are oriented across the slope, but the near-bottom M2 tidal ellipse is smaller in magnitude and strongly indicates enhanced local near-bottom energy dissipation of the barotropic tide through tide–topography interaction (Table 2; Fig. 8). At the LSB site, near-bottom M2 and S2 tidal ellipses from the ADCP are oriented along the slope with a small across-slope component. In contrast, modelled barotropic semidiurnal tidal harmonics were of similar magnitude but mainly oriented across the slope (Table 2; Fig. 8). This discrepancy is likely due to local changes in bathymetry (Fig. S1), which are not resolved in the OTIS tidal model. The outcome of strongly enhanced current speeds at the HSB site is contrary to White (2003), who measured high current speeds in areas where no sponges were recorded, and vice versa, in the Porcupine Seabight. Caution should be applied comparing these areas, as the sponge fields in the Porcupine Seabight mostly consist of glass sponges, whereas we see a mixture of glass sponges and massive demosponges. Bottom current speeds are higher at HSB than at LSB (Table 1), but bottom currents at LSB are still comparable with current speeds found at other sponge grounds on the Scotian Shelf (mean: $0.12\,\mathrm{m\,s^{-1}}$; Hanz et al., 2021a) and on the Arctic Mid-Atlantic Ridge (mean: $0.14\,\mathrm{m\,s^{-1}}$; Hanz et al., 2021b). The conversion of kinetic energy from barotropic to baroclinic tides and to turbulence over rough topography shapes the distribution of benthic filter-feeding communities in many areas throughout the global ocean (van der Kaaden et al., 2024). At the northern Labrador shelf break, larger aggregations of sponges are mainly found on topographic slopes, where near-critical and super-critical reflection of internal waves are predicted (Fig. 13).

4.4 How can strong bottom currents benefit the benthic community?

Strong tidally induced bottom currents can benefit the benthic community at the HSB site in various ways. First, passive suspension feeders (such as the gorgonian *P. resedaeformis*) benefit from high horizontal currents via an increased particulate organic matter (POM) flux (Shimeta and Jumars, 1991), while sponges (specifically glass sponges) could benefit from an increased water flow rate through their body plan (Leys et al., 2011; Vogel, 1977), thereby increasing food availability. Second, resuspension caused by oscillating tidal bottom currents enhance organic matter and inorganic nutrient availability in the benthic boundary layer and enhance food supply to the sponges (Roberts et al., 2018). In this study, high along-slope bottom currents at both sites were

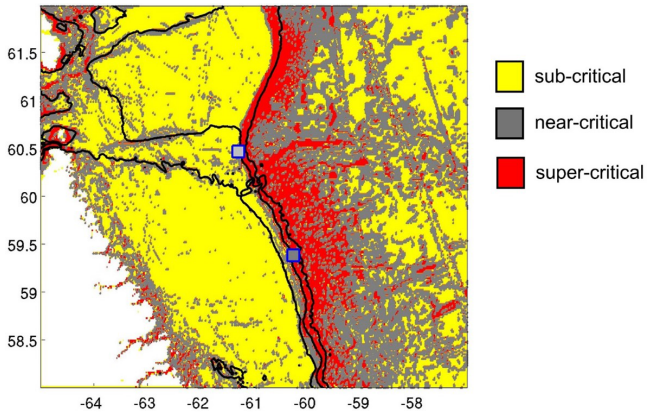

Figure 13. The internal wave slope parameter indicates sub-critical conditions across most of the Labrador Shelf and in the deep northwestern Atlantic. Near-critical and super-critical conditions are primarily observed along the continental margin. This analysis suggests that the HSB lander (northern point) was situated in near-critical conditions for the M2 tide, while the LSB lander (southern point) experienced super-critical bottom slopes for M2.

associated with increased turbidity (both ABS and OBS), indicative of resuspension. However, the beneficial effect of resuspension for sponge biomass is not yet fully understood, as reoccurring strong turbidity flows (at LSB) could also prevent high sponge biomass from developing by smothering young sponges when particles settle out (Klitgaard and Tendal, 2004).

The substrate at HSB consisted mostly of pebbles, cobbles, and boulders (Dinn et al., 2020), whereas a qualitative assessment of the sediment type at LSB suggested the dominance of muddy, soft sediment (Cote, 2020; Johanne Vad, personal communication, 2023). As higher bottom currents would increase bed shear stress and, thus, enhance resuspension (Jones et al., 1998; Lesht, 1979), we argue that fine material is resuspended at HSB before its accumulation on the seafloor. This increases the availability of organic matter to benthic suspension feeders in the benthic boundary layer and prevents smothering from sedimentation. Resuspension has also been linked to high sponge biomass (Davison et al., 2019), as potential food sources such as organic matter and bacteria can bind to suspended particles in the water column. The interaction of high bottom currents with rough topography causes turbulence and mixing of bottom waters (Witte et al., 1997; Leys et al., 2011; Culwick et al., 2020). As the substrate is likely rougher and bottom currents are higher at HSB than at LSB, the bottom water probably experiences more intense mixing and turbulence at HSB. Finally, the periodic supply of fresh phytoplankton-derived material during the spring bloom (Figs. S10, S11) increases food availability for the passive suspension feeders living on the sponge grounds. In short, the stronger tidal currents at HSB enhance bottom-water mixing, replenishing oxygen, dissolved organic matter, POM, and (inorganic) nutrients in the benthic boundary layer and, thus, increasing the food supply for benthic fauna (Davison et al., 2019; Hanz et al., 2021a, b).

4.5 Surface productivity and benthic–pelagic coupling

The Hudson Strait outflow water is known to increase nutrient concentrations in the surface waters on the northern Labrador Shelf (Drinkwater and Harding, 2001; Kollmeyer et al., 1967; Sutcliffe et al., 1983). The increased nutrient supply supports high primary productivity in an area extending from the Hudson Strait to the southern Labrador Shelf, bounded by the thermal front associated with the 1000 m isobath (Cyr and Larouche, 2015; Frajka-Williams et al., 2009; Frajka-Williams and Rhines, 2010). Previous studies have shown that surface Chl-*a* concentrations are comparable between the two sponge grounds (see Fig. 2a in Frajka-Williams and Rhines, 2010), suggesting that differences in surface productivity alone are insufficient to explain the differences in sponge biomass between regions. Furthermore, studies elsewhere in the Canadian Arctic have shown that benthic biomass is explained not only by surface productivity but also by local hydrodynamics and benthic–pelagic coupling (Grebmeier and Barry, 1991; Roy et al., 2014; Thomson, 1982).

Our year-long recordings of bottom-water Chl-*a* concentrations provide evidence of strong benthic–pelagic coupling during spring in this region. The benthic landers showed the early arrival of fresh phytodetritus in early March, a peak in Chl-*a* in mid-April, and a Chl-*a* concentration that was close to background values again from early May at LSB and from mid-May at HSB (Fig. 9c). Studies on the onset of the phytoplankton bloom on the Labrador Shelf show that blooms usually initiate around mid-April and peak around mid-June (Cyr et al., 2023; Frajka-Williams and Rhines, 2010; Fuentes-Yaco et al., 2007). The study of Cyr et al. (2023) estimates that the standard deviation in the timing of the initiation of the phytoplankton bloom is around 21 d. As environmental conditions of the northern Labrador Shelf were close to average during 2019 (Cyr and Galbraith, 2021), we think that it is acceptable to assume that the phytoplankton bloom timing was similar to values found in the literature. Therefore, arrival of phytodetritus at our benthic landers was 3 months earlier than the normal phytoplankton bloom timing. Earlier research has shown that Chl-*a* starts to increase on the northern Labrador Shelf from early March onwards (Harrison et al., 2013). During this time, the water column is still relatively cold and poorly stratified, allowing for relatively high export of phytoplankton to the seafloor. Additionally, the short periods of low ice cover in mid-February and mid-March (Fig. S11d) match the subsequent increase in the bottom Chl-*a* concentration seen for both landers (Fig. 9c). The onset of the phytoplankton bloom for the northern Labrador Shelf is around mid-April and is related to the onset of stratification (Cyr et al., 2023) and

sea-ice cover (Wu et al., 2007). The timing of peak bottom Chl-*a* concentrations (mid-April) and consequential decline compare well with the timing of phytoplankton bloom initiation proposed by Cyr et al. (2023). They show that there is a south-to-north progression of the phytoplankton bloom over the Labrador Shelf; this matches with our data which show that Chl-*a* concentrations stay elevated around 3 weeks longer at the more northern HSB lander. Furthermore, assuming that surface Chl-*a* concentration peaks in June, we can infer that there appears to be a decoupling between pelagic productivity and bottom Chl-*a* concentration in summer, likely due to enhanced stratification and intense zooplankton grazing (Rivkin et al., 1996; Turner, 2015).

Our findings suggest that strong benthic–pelagic coupling started weeks before the peak of the phytoplankton bloom, supplying fresh fluorescent material to the seafloor in spring for a period of weeks to months. As the timing of phytoplankton bloom for high-latitude seas is shifting to earlier in the year due rising temperatures and earlier sea-ice retreat (Edwards and Richardson, 2004; Hunter-Cevera et al., 2016; Wu et al., 2007) and because deep-sea sessile organisms, such as cold-water corals and deep-sea sponges, demonstrate seasonality in their phenology (Leys and Lauzon, 1998; Maier et al., 2020b; Maldonado, 2011), the early arrival of phytoplankton-derived material could have consequences for their overall fitness and survival. Nevertheless, the effect of a shift in the spring bloom timing for benthic suspension feeders, including deep-sea sponges, remains unknown.

Recent ABS measurements have revealed a layer of increased 300 kHz backscatter along the northern Labrador Shelf, indicative of a high abundance of micronekton and macrozooplankton (Chawarski et al., 2022). Earlier studies showed a high zooplankton biomass on the Newfoundland Shelf from July onwards (Head et al., 2003, 2013). In our traps, the highest flux of unsaturated alcohols, a biomarker for zooplankton (specifically copepods; Dalsgaard et al., 2003), and the highest numbers of swimmers were in summer and autumn. During the spring bloom, trapped material at LSB had the highest relative amount of unsaturated alcohols, while the level of PUFAs, markers for phytoplankton derived-material, was highest at HSB (Dalsgaard et al., 2003). Furthermore, our observations suggest that the number of trapped swimmers was higher at LSB than at HSB. These results are consistent with the hypothesis that zooplankton biomass is high over the northern Labrador Shelf (Saglek Bank) and that zooplankton are transported by the southerly current along the Labrador Shelf together with the high phytoplankton biomass plume (Drinkwater and Harding, 2001; Sutcliffe et al., 1983). Overall, there was a larger fraction of zooplankton marker lipids in trapped material at LSB, which implies that zooplankton play a more important role in benthic–pelagic coupling at LSB than at HSB.

4.6 Organic matter fluxes to the seafloor

Organic matter deposition was higher at the HSB lander than at the LSB lander. Overall, deposition was highest during the winter months and consisted of more degraded material than during summer, indicated by high C : N ratios and high δ^{15}N values. This increased deposition in winter is likely resuspended material, as shown by peaks in ABS turbidity in the bottom boundary layer, and is related to higher current speeds. The C : N ratio of deposited matter was higher at LSB (~ 13) compared with HSB (~ 8), indicating that the material was more degraded at LSB. Hanz et al. (2021a, b) also found higher mass and carbon fluxes during winter months and low carbon fluxes when the spring phytoplankton bloom arrived. They attributed this to the presence of more degraded and resuspended material in winter. Data concerning mass fluxes from sponge grounds remain scarce, but the fluxes measured here (HSB $2.46 \pm 1.76\,\mathrm{g\,m^{-2}\,d^{-1}}$; LSB: $1.43 \pm 0.93\,\mathrm{g\,m^{-2}\,d^{-1}}$) were comparable to those of a *Vazella pourtalesii* sponge ground on the Scotian Shelf ($3.17 \pm 3.42\,\mathrm{g\,m^{-2}\,d^{-1}}$; Hanz et al., 2021a) but substantially higher than those of a sponge ground on the Arctic Mid-Atlantic Ridge (0.03–$0.30\,\mathrm{g\,m^{-2}\,d^{-1}}$; Hanz et al., 2021b). Overall, our data suggest that organic matter deposition fluxes are higher at HSB compared with LSB and that the organic matter is of higher quality. The organic carbon fluxes (HSB: $3.07 \pm 1.91\,\mathrm{mmol\,C\,m^{-2}\,d^{-1}}$; LSB: $1.91 \pm 0.71\,\mathrm{mmol\,C\,m^{-2}\,d^{-1}}$) reported in our study are considerably lower than those of a more shallow (150–250 m depth) *V. pourtalesii* sponge ground on the Scotian Shelf ($8.3\,\mathrm{mmol\,C\,m^{-2}\,d^{-1}}$; Hanz et al., 2021a) but high compared with an Arctic Mid-Atlantic Ridge sponge ground (peak of $1.6\,\mathrm{mmol\,C\,m^{-2}\,d^{-1}}$; Hanz et al., 2021b). The higher organic matter deposition rate and relative fresher material at HSB compared with LSB are likely related to its shallower position on the shelf and the more dynamic water column.

4.7 Isotopic signatures of benthic macrofauna at two contrasting sponge grounds

Although the sample size was limited, the stable isotope data revealed interesting patterns of organic matter utilization by the benthic community. The gorgonian coral *P. resedaeformis* is found one trophic level (Fry, 2006) above the sediment trap material and, therefore, likely feeds on sinking organic matter, confirming previous observations (Sherwood et al., 2005, 2008). Sponges can generally be classified into two groups based on their associated microbial fauna: those with high microbial abundance (HMA) or those with low microbial abundance (LMA; Vacelet and Donadey, 1977). *Geodia* spp. can occur in high abundance and biomass on sponge grounds (Kutti et al., 2013). These sponges are considered HMA (Radax et al., 2012) and feed mostly on dissolved organic matter with additional particulate sources, such as bacterioplankton (Bart et al., 2021). Many hexactinellids that

can form sponge grounds, for instance *Vazella pourtalesii* and *Aphrocallistes vastus*, are considered LMA sponges and feed mostly on bacterioplankton (Kahn et al., 2015). The high δ^{15}N isotopic ratios for the sponges *Asconema* spp. (12.6 ± 0.3 ‰ δ^{15}N) and *Mycale* spp. (13.1 ± 0.4 ‰ δ^{15}N) have been observed previously for LMA sponges (Iken et al., 2001; Kahn et al., 2018; Polunin et al., 2001). Deep-sea LMA sponges typically have elevated δ^{15}N values in the benthic food web (Kahn et al., 2018), a phenomenon that is still poorly understood. Possible explanations could be selective feeding on ^{15}N-enriched bacteria (Wilkinson et al., 1984), feeding on resuspended benthic bacteria (Kahn et al., 2018), or nitrogen (re)cycling within the sponge holobiont (Hanz et al., 2022; Rooks et al., 2020). Interestingly, the HMA massive sponge *Geodia* sp. has distinct δ^{13}C and δ^{15}N values, as also observed in Hanz et al. (2022), indicating different feeding or metabolic strategies. Recent research on *Geodia barretti* has indeed demonstrated that these sponges rely in large part on dissolved organic matter (DOM) for their metabolic requirements (Bart et al., 2021; de Kluijver et al., 2021). In this study, *Geodia* spp. (8.2 ± 0.2 ‰ δ^{15}N) was one trophic level higher than oceanic DOM δ^{15}N (~ 5‰; Benner et al., 2005; Sigman et al., 2009) and δ^{15}N-NO_3^- (~ 5‰; Sigman et al., 2009; Sherwood et al., 2021), limiting our ability to distinguish between DOM and NO_3^- (by i.e. denitrification; Hoffmann et al., 2009) as potential nitrogen sources. The δ^{13}C value of *Geodia* spp. (-18.4 ± 0.17 ‰ δ^{13}C) is ± 3.5‰ higher than bottom-water δ^{13}C-DOC values on the Labrador Shelf (Barber et al., 2017), i.e. more than 4 times higher than the expected 0.8 ‰ δ^{13}C step per trophic level (Vander Zanden and Rasmussen, 2001). Alternatively, *Geodia* spp. could capitalize on dissolved inorganic carbon (DIC) via their symbionts (de Kluijver et al., 2021), as recently observed in Arctic *Geodia* spp. assemblages (Morganti et al., 2022) and other deep-sea sponges (van Duyl et al., 2020). Even limited chemoautotrophic assimilation of high-δ^{13}C DIC (~ 0‰ δ^{13}C) could explain the high δ^{13}C values of *Geodia* spp. These results indicate that passive suspension feeders benefit from high tidal currents through an increased particulate organic matter flux (Shimeta and Jumars, 1991), whereas sponges likely benefit from replenishment of nutrients, oxygen, and DOM (Schläppy et al., 2010).

5 Conclusions

The aim this research was to obtain a better understanding of the environmental conditions under which sponge grounds occur and investigate the conditions under which high sponge biomass could develop. This study identified that the high-biomass sponge ground on the northern Labrador Shelf differs from the low-biomass sponge ground in the following ways: a more dynamic water column with strong tidal bottom currents and near-bottom energy dissipation by tide–topography interactions, increased bottom inorganic nutrient concentrations, and higher organic matter flux to the seafloor. Furthermore, both sponge grounds experienced strong benthic–pelagic coupling during spring and a decoupling during summer months. The elevated bottom nutrient concentrations at the high-sponge-biomass ground could be related to large-scale circulation or sediment effluxes, and future work is needed to assess this. Our findings suggest a relation between slope criticality and sponge biomass on the northern Labrador Shelf which could be interesting to investigate in future work. The deep-sea sponges and corals benefit from the dynamic water column in the high-biomass sponge ground via the increased availability of food sources and nutrients.

Data availability. The data pertaining to this work are available from https://doi.org/10.5281/zenodo.10571403 (de Froe et al., 2024).

Supplement. The supplement related to this article is available online at: https://doi.org/10.5194/bg-21-5407-2024-supplement.

Author contributions. EdF: sample analysis, data analysis, and writing; IY: data collection, data analysis, and writing; CM: conceptualization, data analysis, and writing; JV: data collection and data analysis; FM: conceptualization, sample analysis, and data analysis; GD: conceptualization and data analysis; EK, EH, IY, SWR, and JMR: conceptualization and site selection; SWR, JMR, EK, BM, and GT: site contribution and preparation of benthic landers; GAW: conceptualization, sample analysis, data analysis, and writing; SB: data collection and sample analysis; DvO: conceptualization, data analysis, and writing. All authors contributed to the article and approved the submitted version.

Competing interests. The contact author has declared that none of the authors has any competing interests.

Disclaimer. Publisher's note: Copernicus Publications remains neutral with regard to jurisdictional claims made in the text, published maps, institutional affiliations, or any other geographical representation in this paper. While Copernicus Publications makes every effort to include appropriate place names, the final responsibility lies with the authors.

Acknowledgements. We would like to thank the skilful crew and technicians aboard CCGS *Amundsen* for their support during the fieldwork. Specifically, we thank Paul Snelgrove (Memorial University of Newfoundland), Evan Edinger (Memorial University of Newfoundland), David Coté (DFO), and Shawn Meredyk (Amundsen Science) for their assistance with facilitating our field programme. Cam Lirette (DFO) assisted with preparing various data layers to aid with site selection. We would also like to

thank Jan Peene for nutrient analysis; Peter van Breugel and Jurian Brasser for help with measuring macrofauna, POM, and sediment trap stable isotopes; and Pascal Guillot for quality assurance of the CTD profiles. Finally, we thank Kevin MacIsaac and Marc Ringuette for their help with identifying the sediment trap swimmers.

Financial support. This research has been supported by the European Union's Horizon 2020 Research and Innovation programme under grant agreement nos. 678760 (ATLAS) and 818123 (iAtlantic). This output reflects only the authors' view, and the European Union cannot be held responsible for any use that may be made of the information contained therein. The Department of Fisheries and Oceans contributions were funded through the departmental International Governance Strategy programme awarded to Ellen Kenchington. Dick van Oevelen was supported by the Innovational Research Incentives Scheme of the Netherlands Organisation for Scientific Research (NWO) under grant agreement no. 864.13.007. Evert de Froe was partly supported by the ArcticNet Network of Centres of Excellence, "Glacier troughs as biodiversity and abundance hotspots in Arctic and subarctic regions" project, ArcticNet Phase V (Geoffroy et al., 2022). The data presented herein were collected by the Canadian research icebreaker CCGS *Amundsen* and made available by the Amundsen Science programme, which was supported by the Canada Foundation for Innovation and Natural Sciences and Engineering Research Council of Canada. The views expressed in this publication do not necessarily represent the views of Amundsen Science or that of its partners. Ship time on the CCGS *Amundsen* was also funded by an NSERC ship-time grant (Edinger et al., 2018, grant no. RGPST-515528-2018), the ArcticNet Network of Centers of Excellence Canada, and the Department of Fisheries and Oceans Canada (DFO) programs ISICLE and ISECOLD (led by David Coté). The funders had no role in the study design, data collection, or analysis; decision to publish; or preparation of the manuscript.

Review statement. This paper was edited by Andrew Thurber and reviewed by Ulrike Hanz and one anonymous referee.

References

Abelson, A. and Denny, M.: Settlement of Marine Organisms in Flow, Annu. Rev. Ecol. Syst., 28, 317–339, https://doi.org/10.1146/annurev.ecolsys.28.1.317, 1997.

Andrews, D. and Hargrave, B. T.: Close interval sampling of interstitial silicate and porosity in marine sediments, Geochim. Cosmochim. Ac., 48, 711–722, https://doi.org/10.1016/0016-7037(84)90097-8, 1984.

Barber, A., Sirois, M., Chaillou, G., and Gélinas, Y.: Stable isotope analysis of dissolved organic carbon in Canada's eastern coastal waters, Limnol. Oceanogr., 62, S71–S84, https://doi.org/10.1002/lno.10666, 2017.

Bart, M. C., Mueller, B., Rombouts, T., van de Ven, C., Tompkins, G. J., Osinga, R., Brussaard, C. P. D., MacDonald, B., Engel, A., Rapp, H. T., and de Goeij, J. M.: Dissolved organic carbon (DOC) is essential to balance the metabolic demands of four dominant North-Atlantic deep-sea sponges, Limnol. Oceanogr., 66, 925–938, https://doi.org/10.1002/lno.11652, 2021.

Beazley, L., Wang, Z., Kenchington, E., Yashayaev, I., Rapp, H. T., Xavier, J. R., Murillo, F. J., Fenton, D., and Fuller, S.: Predicted distribution of the glass sponge Vazella pourtalesi on the Scotian Shelf and its persistence in the face of climatic variability, PLOS ONE, 13, e0205505, https://doi.org/10.1371/journal.pone.0205505, 2018.

Beazley, L., Kenchington, E., Murillo, F., Brickman, D., Wang, Z., Davies, A., Roberts, E., and Rapp, H.: Climate change winner in the deep sea? Predicting the impacts of climate change on the distribution of the glass sponge Vazella pourtalesii, Mar. Ecol. Prog. Ser., 657, 1–23, https://doi.org/10.3354/meps13566, 2021.

Beazley, L. I., Kenchington, E. L., Murillo, F. J., and del Sacau, M. M.: Deep-sea sponge grounds enhance diversity and abundance of epibenthic megafauna in the Northwest Atlantic, ICES J. Mar. Sci., 70, 1471–1490, https://doi.org/10.1093/icesjms/fst124, 2013.

Becker, R. A., Wilks, A. R., and Brownrigg, R.: R package: Mapdata: Extra Map Databases (Version 2.3.1), CRAN [code], https://CRAN.R-project.org/package=mapdata (last access: 1 December 2023), 2022.

Belkin, I. M.: Rapid warming of Large Marine Ecosystems, Prog. Oceanogr., 81, 207–213, https://doi.org/10.1016/j.pocean.2009.04.011, 2009.

Benner, R., Louchouarn, P., and Amon, R. M. W.: Terrigenous dissolved organic matter in the Arctic Ocean and its transport to surface and deep waters of the North Atlantic, Global Biogeochem. Cy., 11, https://doi.org/10.1029/2004GB002398, 2005.

Bergquist, P. R.: Sponges, University of California Press, 282 pp., ISBN 978-0-520-03658-1, 1978.

Bloomfield, P.: Fourier analysis of time series: an introduction, John Wiley & Sons, https://doi.org/10.1002/0471722235, 2004.

Brito-Morales, I., Schoeman, D. S., Molinos, J. G., Burrows, M. T., Klein, C. J., Arafeh-Dalmau, N., Kaschner, K., Garilao, C., Kesner-Reyes, K., and Richardson, A. J.: Climate velocity reveals increasing exposure of deep-ocean biodiversity to future warming, Nat. Clim. Change, 10, 576–581, https://doi.org/10.1038/s41558-020-0773-5, 2020.

Brodnicke, O. B., Meyer, H. K., Busch, K., Xavier, J. R., Knudsen, S. W., Møller, P. R., Hentschel, U., and Sweet, M. J.: Deep-sea sponge derived environmental DNA analysis reveals demersal fish biodiversity of a remote Arctic ecosystem, Environmental DNA, 5, 1405–1417, https://doi.org/10.1002/edn3.451, 2023.

Buhl-Mortensen, L., Vanreusel, A., Gooday, A. J., Levin, L. A., Priede, I. G., Buhl-Mortensen, P., Gheerardyn, H., King, N. J., and Raes, M.: Biological structures as a source of habitat heterogeneity and biodiversity on the deep ocean margins, Mar, Ecol,, 31, 21–50, https://doi.org/10.1111/j.1439-0485.2010.00359.x, 2010.

Cacchione, D. A., Pratson, L. F., and Ogston, A. S.: The Shaping of Continental Slopes by Internal Tides, Science, 296, 724–727, https://doi.org/10.1126/science.1069803, 2002.

Campitelli, E.: metR: Tools for Easier Analysis of Meteorological Fields, Zenodo, https://doi.org/10.5281/zenodo.2593516, 2021.

Cathalot, C., Van Oevelen, D., Cox, T. J. S., Kutti, T., Lavaleye, M., Duineveld, G., and Meysman, F. J. R.: Cold-water coral reefs and adjacent sponge grounds: hotspots of benthic respiration and

organic carbon cycling in the deep sea, Front. Mar. Sci., 2, 37, https://doi.org/10.3389/fmars.2015.00037, 2015.

Centurioni, L. R., Turton, J., Lumpkin, R., Braasch, L., Brassington, G., Chao, Y., Charpentier, E., Chen, Z., Corlett, G., Dohan, K., Donlon, C., Gallage, C., Hormann, V., Ignatov, A., Ingleby, B., Jensen, R., Kelly-Gerreyn, B. A., Koszalka, I. M., Lin, X., Lindstrom, E., Maximenko, N., Merchant, C. J., Minnett, P., O'Carroll, A., Paluszkiewicz, T., Poli, P., Poulain, P.-M., Reverdin, G., Sun, X., Swail, V., Thurston, S., Wu, L., Yu, L., Wang, B., and Zhang, D.: Global in situ Observations of Essential Climate and Ocean Variables at the Air–Sea Interface, Front. Mar. Sci., 6, https://doi.org/10.3389/fmars.2019.00419, 2019.

Chawarski, J., Klevjer, T. A., Coté, D., and Geoffroy, M.: Evidence of temperature control on mesopelagic fish and zooplankton communities at high latitudes, Front. Mar. Sci., 9, https://doi.org/10.3389/fmars.2022.917985, 2022.

Christie, W. W.: A simple procedure for rapid transmethylation of glycerolipids and cholesteryl esters, J. Lipid Res., 23, 1072–1075, https://doi.org/10.1016/S0022-2275(20)38081-0, 1982.

Colaço, A., Rapp, H. T., Campanyà-Llovet, N., and Pham, C. K.: Bottom trawling in sponge grounds of the Barents Sea (Arctic Ocean): A functional diversity approach, Deep-Sea Res. Pt. I, 183, 103742, https://doi.org/10.1016/j.dsr.2022.103742, 2022.

Cote, D.: Cruise report – Integrated Studies and Ecosystem Characterization of the Labrador Sea Deep Ocean (ISECOLD), Zenodo, https://doi.org/10.5281/zenodo.3862120, 2020.

Coté, D., Edinger, E. N., and Mercier, A.: CCGS Amundsen Field Report. Integrated studies and ecosystem characterization of the Labrador Sea Deep Ocean (ISECOLD), p. 41, https://amundsenscience.com/expeditions/2018-expedition/ (last access: 3 December 2024), 2018.

Culwick, T., Phillips, J., Goodwin, C., Rayfield, E. J., and Hendry, K. R.: Sponge Density and Distribution Constrained by Fluid Forcing in the Deep Sea, Front. Mar. Sci., 7, 395, https://doi.org/10.3389/fmars.2020.00395, 2020.

Cuny, J., Rhines, P. B., Niiler, P. P., and Bacon, S.: Labrador Sea Boundary Currents and the Fate of the Irminger Sea Water, J. Phys. Oceanogr., 32, 627–647, https://doi.org/10.1175/1520-0485(2002)032<0627:LSBCAT>2.0.CO;2, 2002.

Curry, B., Lee, C. M., and Petrie, B.: Volume, Freshwater, and Heat Fluxes through Davis Strait, 2004–05, J. Phys. Oceanogr., 41, 429–436, https://doi.org/10.1175/2010JPO4536.1, 2011.

Curry, B., Lee, C. M., Petrie, B., Moritz, R. E., and Kwok, R.: Multiyear Volume, Liquid Freshwater, and Sea Ice Transports through Davis Strait, 2004–10, J. Phys. Oceanogr., 44, 1244–1266, https://doi.org/10.1175/JPO-D-13-0177.1, 2014.

Cyr, F. and Galbraith, P. S.: A climate index for the Newfoundland and Labrador shelf, Earth Syst. Sci. Data, 13, 1807–1828, https://doi.org/10.5194/essd-13-1807-2021, 2021.

Cyr, F. and Larouche, P.: Thermal Fronts Atlas of Canadian Coastal Waters, Atmos. Ocean, 53, 212–236, https://doi.org/10.1080/07055900.2014.986710, 2015.

Cyr, F., Lewis, K., Bélanger, D., Regular, P., Clay, S., and Devred, E.: Physical controls and ecological implications of the timing of the spring phytoplankton bloom on the Newfoundland and Labrador shelf, Limnol. Oceanogr. Lett., 9, 191–198, https://doi.org/10.1002/lol2.10347, 2023.

Dalsgaard, J., St. John, M., Kattner, G., Müller-Navarra, D., and Hagen, W.: Fatty acid trophic markers in the pelagic marine environment, in: Advances in Marine Biology, vol. 46, Elsevier, 225–340, https://doi.org/10.1016/S0065-2881(03)46005-7, 2003.

Davison, J. J., van Haren, H., Hosegood, P., Piechaud, N., and Howell, K. L.: The distribution of deep-sea sponge aggregations (Porifera) in relation to oceanographic processes in the Faroe-Shetland Channel, Deep-Sea Res. Pt. I, 146, 55–61, https://doi.org/10.1016/j.dsr.2019.03.005, 2019.

de Froe, E., Yashayaev, I., Mohn, C., Vad, J., Mienis, F., Duineveld, G., Kenchington, E., Head, E., Ross, S. W., Blackbird, S., Wolff, G. A., Roberts, M., MacDonald, B. W., Tulloch, G., and van Oevelen, D.: Supplementary data to: Characterizing regional oceanography and bottom environmental conditions at two contrasting sponge grounds on the northern Labrador Shelf, Zenodo [data set], https://doi.org/10.5281/zenodo.10571403, 2024.

de Kluijver, A., Bart, M. C., van Oevelen, D., de Goeij, J. M., Leys, S. P., Maier, S. R., Maldonado, M., Soetaert, K., Verbiest, S., and Middelburg, J. J.: An Integrative Model of Carbon and Nitrogen Metabolism in a Common Deep-Sea Sponge (Geodia barretti), Front. Mar. Sci., 7, 1131, https://doi.org/10.3389/fmars.2020.596251, 2021.

Dinn, C., Zhang, X., Edinger, E., and Leys, S. P.: Sponge communities in the eastern Canadian Arctic: species richness, diversity and density determined using targeted benthic sampling and underwater video analysis, Polar Biol., 43, 1287–1305, https://doi.org/10.1007/s00300-020-02709-z, 2020.

Drinkwater, K. F. and Harding, G. C.: Effects of the Hudson Strait outflow on the biology of the Labrador Shelf, Can. J. Fish. Aquat. Sci., 58, 171–184, https://doi.org/10.1139/f00-210, 2001.

Drinkwater, K. F. and Jones, E. P.: Density stratification, nutrient and chlorophyll distributions in the Hudson Strait region during summer and their relation to tidal mixing, Cont. Shelf Res., 7, 599–607, https://doi.org/10.1016/0278-4343(87)90025-2, 1987.

Dunbar, M. J.: Eastern Arctic waters: a summary of our present knowledge of the physical oceanography of the eastern arctic area, from Hudson bay to cape Farewell and from Bell Isle to Smith sound, Fisheries Research Board of Canada, Ottawa, 131 pp., https://waves-vagues.dfo-mpo.gc.ca/library-bibliotheque/10206.pdf (last access: 3 December 2024), 1951.

Edwards, M. and Richardson, A. J.: Impact of climate change on marine pelagic phenology and trophic mismatch, Nature, 430, 881–884, https://doi.org/10.1038/nature02808, 2004.

Egbert, G. D. and Erofeeva, S. Y.: Efficient Inverse Modeling of Barotropic Ocean Tides, J. Atmos. Ocean. Technol., 19, 183–204, https://doi.org/10.1175/1520-0426(2002)019<0183:EIMOBO>2.0.CO;2, 2002.

Elipot, S., Lumpkin, R., Perez, R. C., Lilly, J. M., Early, J. J., and Sykulski, A. M.: A global surface drifter data set at hourly resolution, J. Geophys. Res.-Oceans, 121, 2937–2966, https://doi.org/10.1002/2016JC011716, 2016.

Elipot, S., Sykulski, A. M., Lumpkin, R., Centurioni, L. R., and Pazos, M.: Hourly location, current velocity, and temperature collected from Global Drifter Program drifters world-wide, NOAA National Centers for Environmental Information [data set], https://doi.org/10.25921/x46c-3620, 2022.

Fissel, D. B. and Lemon, D. D.: Analysis of physical oceanographic data from the Labrador Shelf, summer 1980, No. 39, Canadian Contractor Report of Hydrography and Ocean Sciences, 136

pp., Bedford Institute of Oceanography. https://www.osti.gov/etdeweb/biblio/5105285 (last access: 3 December 2024), 1991.

Frajka-Williams, E. and Rhines, P. B.: Physical controls and interannual variability of the Labrador Sea spring phytoplankton bloom in distinct regions, Deep-Sea Res. Pt. I, 57, 541–552, https://doi.org/10.1016/j.dsr.2010.01.003, 2010.

Frajka-Williams, E., Rhines, P. B., and Eriksen, C. C.: Physical controls and mesoscale variability in the Labrador Sea spring phytoplankton bloom observed by Seaglider, Deep-Sea Res. Pt. I, 56, 2144–2161, https://doi.org/10.1016/j.dsr.2009.07.008, 2009.

Fry, B.: Stable Isotope Ecology, Springer-Verlag, New York, https://doi.org/10.1007/0-387-33745-8, 2006.

Fuentes-Yaco, C., Koeller, P. A., Sathyendranath, S., and Platt, T.: Shrimp (Pandalus borealis) growth and timing of the spring phytoplankton bloom on the Newfoundland–Labrador Shelf, Fish. Oceanogr., 16, 116–129, https://doi.org/10.1111/j.1365-2419.2006.00402.x, 2007.

GEBCO Bathymetric Compilation Group: The GEBCO_2023 Grid – a continuous terrain model of the global oceans and land, [data set], https://doi.org/10.5285/f98b053b-0cbc-6c23-e053-6c86abc0af7b, 2023.

Gille, S. T., Metzger, E. J., and Tokmakian: Seafloor Topography and Ocean Circulation, Oceanography, 17, 47–54, https://doi.org/10.5670/oceanog.2004.66, 2004.

Grebmeier, J. M. and Barry, J. P.: The influence of oceanographic processes on pelagic-benthic coupling in polar regions: A benthic perspective, J. Mar. Syst., 2, 495–518, https://doi.org/10.1016/0924-7963(91)90049-Z, 1991.

Griffiths, D. K., Pingree, R. D., and Sinclair, M.: Summer tidal fronts in the near-arctic regions of Foxe Basin and Hudson Bay, Deep-Sea Res. Pt. I, 28, 865–873, https://doi.org/10.1016/S0198-0149(81)80006-4, 1981.

Grolemund, G. and Wickham, H.: Dates and Times Made Easy with lubridate, J. Stat. Softw., 40, 1–25, 2011.

Guillot, P.: Cruise Bright/SN/Atlas 1802 (leg 2) CTD processing notes, Amundsen Science, 2018.

Haalboom, S., de Stigter, H., Duineveld, G., van Haren, H., Reichart, G.-J., and Mienis, F.: Suspended particulate matter in a submarine canyon (Whittard Canyon, Bay of Biscay, NE Atlantic Ocean): Assessment of commonly used instruments to record turbidity, Mar. Geol., 434, 106439, https://doi.org/10.1016/j.margeo.2021.106439, 2021.

Haalboom, S., de Stigter, H. C., Mohn, C., Vandorpe, T., Smit, M., de Jonge, L., and Reichart, G.-J.: Monitoring of a sediment plume produced by a deep-sea mining test in shallow water, Málaga Bight, Alboran Sea (southwestern Mediterranean Sea), Mar. Geol., 456, 106971, https://doi.org/10.1016/j.margeo.2022.106971, 2023.

Hanz, U., Roberts, E. M., Duineveld, G., Davies, A., Haren, H. van, Rapp, H. T., Reichart, G.-J., and Mienis, F.: Long-term Observations Reveal Environmental Conditions and Food Supply Mechanisms at an Arctic Deep-Sea Sponge Ground, J. Geophys. Res.-Oceans, 126, e2020JC016776, https://doi.org/10.1029/2020JC016776, 2021a.

Hanz, U., Beazley, L., Kenchington, E., Duineveld, G., Rapp, H. T., and Mienis, F.: Seasonal Variability in Near-bed Environmental Conditions in the Vazella pourtalesii Glass Sponge Grounds of the Scotian Shelf, Front. Mar. Sci., 7, 597682, https://doi.org/10.3389/fmars.2020.597682, 2021b.

Hanz, U., Riekenberg, P., de Kluijver, A., van der Meer, M., Middelburg, J. J., de Goeij, J. M., Bart, M. C., Wurz, E., Colaço, A., Duineveld, G. C. A., Reichart, G.-J., Rapp, H.-T., and Mienis, F.: The important role of sponges in carbon and nitrogen cycling in a deep-sea biological hotspot, Funct. Ecol., 36, 2188–2199, https://doi.org/10.1111/1365-2435.14117, 2022.

Harrison, G. W., Yngve Børsheim, K., Li, W. K. W., Maillet, G. L., Pepin, P., Sakshaug, E., Skogen, M. D., and Yeats, P. A.: Phytoplankton production and growth regulation in the Subarctic North Atlantic: A comparative study of the Labrador Sea-Labrador/Newfoundland shelves and Barents/Norwegian/-Greenland seas and shelves, Prog. Oceanogr., 114, 26–45, https://doi.org/10.1016/j.pocean.2013.05.003, 2013.

Head, E. J. H., Harris, L. R., and Yashayaev, I.: Distributions of Calanus spp. and other mesozooplankton in the Labrador Sea in relation to hydrography in spring and summer (1995–2000), Prog. Oceanogr., 59, 1–30, https://doi.org/10.1016/S0079-6611(03)00111-3, 2003.

Head, E. J. H., Melle, W., Pepin, P., Bagøien, E., and Broms, C.: On the ecology of Calanus finmarchicus in the Subarctic North Atlantic: A comparison of population dynamics and environmental conditions in areas of the Labrador Sea-Labrador/Newfoundland Shelf and Norwegian Sea Atlantic and Coastal Waters, Prog. Oceanogr., 114, 46–63, https://doi.org/10.1016/j.pocean.2013.05.004, 2013.

Hijmans, R. J.: terra: Spatial Data Analysis, CRAN [code], https://doi.org/10.32614/CRAN.package.terra, 2023.

Hoffmann, F., Radax, R., Woebken, D., Holtappels, M., Lavik, G., Rapp, H. T., Schläppy, M.-L., Schleper, C., and Kuypers, M. M. M.: Complex nitrogen cycling in the sponge Geodia barretti, Environ. Microb., 11, 2228–2243, https://doi.org/10.1111/j.1462-2920.2009.01944.x, 2009.

Hogg, M. M., Tendal, O. S., Conway, K. W., Pomponi, S. A., Soest, R. W. M. van, Gutt, J., Krautter, M., and Roberts, J. M.: Deep-Sea Sponge Grounds: Reservoirs of Biodiversity, in Cambridge: World Conservation Monitoring Centre, UNEP regional seas report and studies, no. 189, UNEP-WCMC Biodiversity Series, 32, 2010.

Howell, K.-L., Piechaud, N., Downie, A.-L., and Kenny, A.: The distribution of deep-sea sponge aggregations in the North Atlantic and implications for their effective spatial management, Deep-Sea Res. Pt. I, 115, 309–320, https://doi.org/10.1016/j.dsr.2016.07.005, 2016.

Hunter-Cevera, K. R., Neubert, M. G., Olson, R. J., Solow, A. R., Shalapyonok, A., and Sosik, H. M.: Physiological and ecological drivers of early spring blooms of a coastal phytoplankter, Science, 354, 326–329, https://doi.org/10.1126/science.aaf8536, 2016.

Iken, K., Brey, T., Wand, U., Voigt, J., and Junghans, P.: Food web structure of the benthic community at the Porcupine Abyssal Plain (NE Atlantic): a stable isotope analysis, Prog. Oceanogr., 50, 383–405, https://doi.org/10.1016/S0079-6611(01)00062-3, 2001.

Jones, E. P., Dyrssen, D., and Coote, A. R.: Nutrient Regeneration in Deep Baffin Bay with Consequences for Measurements of the Conservative Tracer NO and Fossil Fuel CO_2 in the Oceans, Can. J. Fish. Aquat. Sci., 41, 30–35, https://doi.org/10.1139/f84-003, 1984.

Jones, S. E., Jago, C. F., Bale, A. J., Chapman, D., Howland, R. J. M., and Jackson, J.: Aggregation and resuspension of suspended particulate matter at a seasonally stratified site in the southern North Sea: physical and biological controls, Cont. Shelf Res., 18, 1283–1309, https://doi.org/10.1016/S0278-4343(98)00044-2, 1998.

Jorda, G., Marbà, N., Bennett, S., Santana-Garcon, J., Agusti, S., and Duarte, C. M.: Ocean warming compresses the three-dimensional habitat of marine life, Nat. Ecol. Evol., 4, 109–114, https://doi.org/10.1038/s41559-019-1058-0, 2020.

Kahn, A. S., Yahel, G., Chu, J. W. F., Tunnicliffe, V., and Leys, S. P.: Benthic grazing and carbon sequestration by deep-water glass sponge reefs: Deep-water glass sponge reefs, Limnol. Oceanogr., 60, 78–88, https://doi.org/10.1002/lno.10002, 2015.

Kahn, A. S., Chu, J. W. F., and Leys, S. P.: Trophic ecology of glass sponge reefs in the Strait of Georgia, British Columbia, Sci. Rep., 8, 756, https://doi.org/10.1038/s41598-017-19107-x, 2018.

Kazanidis, G., van Oevelen, D., Veuger, B., and Witte, U. F. M.: Unravelling the versatile feeding and metabolic strategies of the cold-water ecosystem engineer Spongosorites coralliophaga (Stephens, 1915), Deep-Sea Res. Pt. I, 141, 71–82, https://doi.org/10.1016/j.dsr.2018.07.009, 2018.

Kelley, D. and Richards, C.: oce: Analysis of Oceanographic Data, CRAN [code], https://doi.org/10.32614/CRAN.package.oce, 2020.

Kenchington, E., Power, D., and Koen-Alonso, M.: Associations of demersal fish with sponge grounds on the continental slopes of the northwest Atlantic, Mar. Ecol. Prog. Ser., 477, 217–230, https://doi.org/10.3354/meps10127, 2013.

Kenchington, E., Yashayaev, I., Tendal, O. S., and Jørgensbye, H.: Water mass characteristics and associated fauna of a recently discovered Lophelia pertusa (Scleractinia: Anthozoa) reef in Greenlandic waters, Polar Biol., 40, 321–337, https://doi.org/10.1007/s00300-016-1957-3, 2017.

Kenchington, E. L., Lirette, C., Cogswell, A., Archambault, D., Archambault, P., Benoit, H., Bernier, D., Brodie, B., Fuller, S., Gilkinson, K., Lévesque, M., Power, D., Siferd, T., Treble, M., and Wareham, V.: Delineating Coral and Sponge Concentrations in the Biogeographic Regions of the East Coast of Canada Using Spatial Analyses, DFO Can. Sci. Advis. Sec. Res. Doc., vi + 202 pp., 2010.

Kieke, D. and Yashayaev, I.: Studies of Labrador Sea Water formation and variability in the subpolar North Atlantic in the light of international partnership and collaboration, Prog. Oceanogr., 132, 220–232, https://doi.org/10.1016/j.pocean.2014.12.010, 2015.

Kiriakoulakis, K., Bett, B. J., White, M., and Wolff, G. A.: Organic biogeochemistry of the Darwin Mounds, a deep-water coral ecosystem, of the NE Atlantic, Deep-Sea Res. Pt. I, 51, 1937–1954, https://doi.org/10.1016/j.dsr.2004.07.010, 2004.

Klitgaard, A. B.: The fauna associated with outer shelf and upper slope sponges (Porifera, Demospongiae) at the Faroe Islands, northeastern Atlantic, Sarsia, 80, 1–22, https://doi.org/10.1080/00364827.1995.10413574, 1995.

Klitgaard, A. B. and Tendal, O. S.: Distribution and species composition of mass occurrences of large-sized sponges in the northeast Atlantic, Prog. Oceanogr., 61, 57–98, https://doi.org/10.1016/j.pocean.2004.06.002, 2004.

Knudby, A., Kenchington, E., and Murillo, F. J.: Modeling the Distribution of Geodia Sponges and Sponge Grounds in the Northwest Atlantic, PLoS ONE, 8, e82306, https://doi.org/10.1371/journal.pone.0082306, 2013.

Kollmeyer, R. C., McGill, D. A., and Corwin, N.: Oceanography of the Labrador Sea in the vicinity of Hudson Strait in 1965, Washington, D.C., U.S. Coast Guard Oceanographic Unit, 108 pp., https://doi.org/10.5962/bhl.title.16966, 1967.

Kutti, T., Bannister, R. J., and Fosså, J. H.: Community structure and ecological function of deep-water sponge grounds in the Traenadypet MPA–Northern Norwegian continental shelf, Cont. Shelf Res., 69, 21–30, https://doi.org/10.1016/j.csr.2013.09.011, 2013.

Kutti, T., Fosså, J., and Bergstad, O.: Influence of structurally complex benthic habitats on fish distribution, Mar. Ecol. Prog. Ser., 520, 175–190, https://doi.org/10.3354/meps11047, 2015.

Canadian Ice Service: Latest Ice conditions, https://www.canada.ca/en/environment-climate-change/services/ice-forecasts-observations/latest-conditions.html (last access: 2 January 2022), 2022.

Lazier, J.: Seasonal variability of temperature and salinity in the Labrador Current, J. Marine Res., 40, https://elischolar.library.yale.edu/journal_of_marine_research/1647, 1982.

Lazier, J., Hendry, R., Clarke, A., Yashayaev, I., and Rhines, P.: Convection and restratification in the Labrador Sea, 1990–2000, Deep-Sea Res. Pt. I, 49, 1819–1835, https://doi.org/10.1016/S0967-0637(02)00064-X, 2002.

Lehmann, N., Kienast, M., Granger, J., Bourbonnais, A., Altabet, M. A., and Tremblay, J.-É.: Remote Western Arctic Nutrients Fuel Remineralization in Deep Baffin Bay, Global Biogeochem. Cy., 33, 649–667, https://doi.org/10.1029/2018GB006134, 2019.

Lesht, B. M.: Relationship between sediment resuspension and the statistical frequency distribution of bottom shear stress, Mar. Geol., 32, M19–M27, https://doi.org/10.1016/0025-3227(79)90142-7, 1979.

Leys, S. P. and Lauzon, N. R. J.: Hexactinellid sponge ecology: growth rates and seasonality in deep water sponges, J. Exp. Mar. Biol. Ecol., 230, 111–129, https://doi.org/10.1016/S0022-0981(98)00088-4, 1998.

Leys, S. P., Yahel, G., Reidenbach, M. A., Tunnicliffe, V., Shavit, U., and Reiswig, H. M.: The Sponge Pump: The Role of Current Induced Flow in the Design of the Sponge Body Plan, PLoS ONE, 6, e27787, https://doi.org/10.1371/journal.pone.0027787, 2011.

López-Acosta, M., Leynaert, A., and Maldonado, M.: Silicon consumption in two shallow-water sponges with contrasting biological features, Limnol. Oceanogr., 61, 2139–2150, https://doi.org/10.1002/lno.10359, 2016.

Maier, S. R., Kutti, T., Bannister, R. J., Fang, J. K.-H., van Breugel, P., van Rijswijk, P., and van Oevelen, D.: Recycling pathways in cold-water coral reefs: Use of dissolved organic matter and bacteria by key suspension feeding taxa, Sci. Rep., 10, 9942, https://doi.org/10.1038/s41598-020-66463-2, 2020a.

Maier, S. R., Bannister, R. J., van Oevelen, D., and Kutti, T.: Seasonal controls on the diet, metabolic activity, tissue reserves and growth of the cold-water coral *Lophelia pertusa*, Coral Reefs, 39, 173–187, https://doi.org/10.1007/s00338-019-01886-6, 2020b.

Maldonado, M.: The ecology of the sponge larva, Can. J. Zool., 84, 175–194, https://doi.org/10.1139/z05-177, 2011.

Maldonado, M., Navarro, L., Grasa, A., Gonzalez, A., and Vaquerizo, I.: Silicon uptake by sponges: a twist to understanding nutrient cycling on continental margins, Sci. Rep., 1, 30, https://doi.org/10.1038/srep00030, 2011.

Maldonado, M., Ribes, M., and van Duyl, F. C.: Nutrient Fluxes Through Sponges, in: Advances in Marine Biology, vol. 62, Elsevier, 113–182, https://doi.org/10.1016/B978-0-12-394283-8.00003-5, 2012.

Maldonado, M., López-Acosta, M., Beazley, L., Kenchington, E., Koutsouveli, V., and Riesgo, A.: Cooperation between passive and active silicon transporters clarifies the ecophysiology and evolution of biosilicification in sponges, Sci. Adv., 6, eaba9322, https://doi.org/10.1126/sciadv.aba9322, 2020a.

Maldonado, M., Beazley, L., López-Acosta, M., Kenchington, E., Casault, B., Hanz, U., and Mienis, F.: Massive silicon utilization facilitated by a benthic-pelagic coupled feedback sustains deep-sea sponge aggregations, Limnol. Oceanogr., 66, 11610, https://doi.org/10.1002/lno.11610, 2020b.

MATLAB: version 7.10.0 (R2010a), The MathWorks Inc., Natick, Massachusetts, https://www.mathworks.com (last access: 3 December 2024), 2010.

McIntyre, F. D., Drewery, J., Eerkes-Medrano, D., and Neat, F. C.: Distribution and diversity of deep-sea sponge grounds on the Rosemary Bank Seamount, NE Atlantic, Mar. Biol., 163, 143, https://doi.org/10.1007/s00227-016-2913-z, 2016.

Meyer, H. K., Roberts, E. M., Rapp, H. T., and Davies, A. J.: Spatial patterns of arctic sponge ground fauna and demersal fish are detectable in autonomous underwater vehicle (AUV) imagery, Deep-Sea Res. Pt. I, 153, 103137, https://doi.org/10.1016/j.dsr.2019.103137, 2019.

Miatta, M. and Snelgrove, P. V. R.: Benthic nutrient fluxes in deep-sea sediments within the Laurentian Channel MPA (eastern Canada): The relative roles of macrofauna, environment, and sea pen octocorals, Deep-Sea Res. Pt. I, 178, 103655, https://doi.org/10.1016/j.dsr.2021.103655, 2021.

Michna, P. and Woods, M.: RNetCDF: Interface to "NetCDF" Datasets, CRAN [code], https://doi.org/10.32614/CRAN.package.RNetCDF, 2019.

Mienis, F., Duineveld, G. C. A., Davies, A. J., Ross, S. W., Seim, H., Bane, J., and van Weering, T. C. E.: The influence of near-bed hydrodynamic conditions on cold-water corals in the Viosca Knoll area, Gulf of Mexico, Deep-Sea Res. Pt. I, 60, 32–45, https://doi.org/10.1016/j.dsr.2011.10.007, 2012.

Morganti, T. M., Slaby, B. M., de Kluijver, A., Busch, K., Hentschel, U., Middelburg, J. J., Grotheer, H., Mollenhauer, G., Dannheim, J., Rapp, H. T., Purser, A., and Boetius, A.: Giant sponge grounds of Central Arctic seamounts are associated with extinct seep life, Nat. Commun., 13, 638, https://doi.org/10.1038/s41467-022-28129-7, 2022.

Morrison, K. M., Meyer, H. K., Roberts, E. M., Rapp, H. T., Colaço, A., and Pham, C. K.: The First Cut Is the Deepest: Trawl Effects on a Deep-Sea Sponge Ground Are Pronounced Four Years on, Front. Mar. Sci., 7, https://doi.org/10.3389/fmars.2020.605281, 2020.

Müller, K. and Wickham, H.: tibble: Simple Data Frames, CRAN [code], https://doi.org/10.32614/CRAN.package.tibble, 2023.

Murillo, F., Kenchington, E., Tompkins, G., Beazley, L., Baker, E., Knudby, A., and Walkusz, W.: Sponge assemblages and predicted archetypes in the eastern Canadian Arctic, Mar. Ecol. Prog. Ser., 597, 115–135, https://doi.org/10.3354/meps12589, 2018.

Murillo, F. J., Muñoz, P. D., Cristobo, J., Ríos, P., González, C., Kenchington, E., and Serrano, A.: Deep-sea sponge grounds of the Flemish Cap, Flemish Pass and the Grand Banks of Newfoundland (Northwest Atlantic Ocean): Distribution and species composition, Mar. Biol. Res., 8, 842–854, https://doi.org/10.1080/17451000.2012.682583, 2012.

Myers, R. A., Akenhead, S. A., and Drinkwater, K.: The influence of Hudson Bay runoff and ice-melt on the salinity of the inner Newfoundland Shelf, Atmos.-Ocean, 28, 241–256, https://doi.org/10.1080/07055900.1990.9649377, 1990.

Neuwirth, E.: RColorBrewer: ColorBrewer Palettes, CRAN [code], https://doi.org/10.32614/CRAN.package.RColorBrewer, 2014.

Newton, P. P., Lampitt, R. S., Jickells, T. D., King, P., and Boutle, C.: Temporal and spatial variability of biogenic particles fluxes during the JGOFS northeast Atlantic process studies at 47° N, 20° W, Deep-Sea Res. Pt. I, 41, 1617–1642, https://doi.org/10.1016/0967-0637(94)90065-5, 1994.

Pedersen, T. L.: patchwork: The Composer of Plots, CRAN [code], https://doi.org/10.32614/CRAN.package.patchwork, 2019.

Petrie, B., Akenhead, S. A., Lazier, J., and Loder, J.: The cold intermediate layer on the Labrador and Northeast Newfoundland Shelves, 1978–86, No. 12, NAFO Science Council Studies, 57–69, 1988.

Pham, C. K., Murillo, F. J., Lirette, C., Maldonado, M., Colaço, A., Ottaviani, D., and Kenchington, E.: Removal of deep-sea sponges by bottom trawling in the Flemish Cap area: conservation, ecology and economic assessment, Sci. Rep., 9, 15843, https://doi.org/10.1038/s41598-019-52250-1, 2019.

Pile, A. J. and Young, C. M.: The natural diet of a hexactinellid sponge: Benthic–pelagic coupling in a deep-sea microbial food web, Deep-Sea Res. Pt. I, 53, 1148–1156, https://doi.org/10.1016/j.dsr.2006.03.008, 2006.

Polunin, N. V. C., Morales-Nin, B., Pawsey, W. E., Cartes, J. E., Pinnegar, J. K., and Moranta, J.: Feeding relationships in Mediterranean bathyal assemblages elucidated by stable nitrogen and carbon isotope data, Mar. Ecol. Prog. Ser., 220, 13–23, https://doi.org/10.3354/meps220013, 2001.

Puerta, P., Johnson, C., Carreiro-Silva, M., Henry, L.-A., Kenchington, E., Morato, T., Kazanidis, G., Rueda, J. L., Urra, J., Ross, S., Wei, C.-L., González-Irusta, J. M., Arnaud-Haond, S., and Orejas, C.: Influence of Water Masses on the Biodiversity and Biogeography of Deep-Sea Benthic Ecosystems in the North Atlantic, Front. Mar. Sci., 7, 239, https://doi.org/10.3389/fmars.2020.00239, 2020.

R Core Team: R: A Language and Environment for Statistical Computing, R Foundation for Statistical Computing, Vienna, Austria, URL https://www.R-project.org/ (last access: 3 December 2024), 2019.

Radax, R., Rattei, T., Lanzen, A., Bayer, C., Rapp, H. T., Urich, T., and Schleper, C.: Metatranscriptomics of the marine sponge Geodia barretti: tackling phylogeny and function of its microbial community, Environ. Microb., 14, 1308–1324, https://doi.org/10.1111/j.1462-2920.2012.02714.x, 2012.

Ricketts, N. B., Trask, P. D., Smith, E. H., Soule, F. M., and Mosby, O.: The "Marion" expedition to Davis Strait and Baffin Bay: Under direction of the United States Coast Guard, 1928, Scien-

tific results: pt.1. Washington, U.S. Govt. Print. Off, 1931–1937, https://doi.org/10.5962/bhl.title.10182, 1931.

Rivkin, R. B., Legendre, L., Deibel, D., Tremblay, J.-É., Klein, B., Crocker, K., Roy, S., Silverberg, N., Lovejoy, C., Mesplé, F., Romero, N., Anderson, M. R., Matthews, P., Savenkoff, C., Vézina, A., Therriault, J.-C., Wesson, J., Bérubé, C., and Ingram, R. G.: Vertical Flux of Biogenic Carbon in the Ocean: Is There Food Web Control?, Science, 272, 1163–1166, https://doi.org/10.1126/science.272.5265.1163, 1996.

Rix, L., de Goeij, J. M., Mueller, C. E., Struck, U., Middelburg, J. J., van Duyl, F. C., Al-Horani, F. A., Wild, C., Naumann, M. S., and van Oevelen, D.: Coral mucus fuels the sponge loop in warm- and cold-water coral reef ecosystems, Sci. Rep., 6, 18715, https://doi.org/10.1038/srep18715, 2016.

Roberts, E. M., Mienis, F., Rapp, H. T., Hanz, U., Meyer, H. K., and Davies, A. J.: Oceanographic setting and short-timescale environmental variability at an Arctic seamount sponge ground, Deep-Sea Res. Pt. I, 138, 98–113, https://doi.org/10.1016/j.dsr.2018.06.007, 2018.

Robertson, L. M., Hamel, J.-F., and Mercier, A.: Feeding in deep-sea demosponges: Influence of abiotic and biotic factors, Deep-Sea Res. Pt. I, 127, 49–56, https://doi.org/10.1016/j.dsr.2017.07.006, 2017.

Rooks, C., Fang, J. K.-H., Mørkved, P. T., Zhao, R., Rapp, H. T., Xavier, J. R., and Hoffmann, F.: Deep-sea sponge grounds as nutrient sinks: denitrification is common in boreo-Arctic sponges, Biogeosciences, 17, 1231–1245, https://doi.org/10.5194/bg-17-1231-2020, 2020.

Roy, V., Iken, K., and Archambault, P.: Environmental Drivers of the Canadian Arctic Megabenthic Communities, PLOS ONE, 9, e100900, https://doi.org/10.1371/journal.pone.0100900, 2014.

Ryan, J. A. and Ulrich, J. M.: xts: eXtensible Time Series, CRAN [code], https://doi.org/10.32614/CRAN.package.xts, 2024.

Schläppy, M.-L., Weber, M., Mendola, D., Hoffmann, F., and de Beer, D.: Heterogeneous oxygenation resulting from active and passive flow in two Mediterranean sponges, Dysida avara and Chondrosia reniformis, Limnol. Oceanogr., 55, 1289–1300, https://doi.org/10.4319/lo.2010.55.3.1289, 2010.

Sherwood, O. A., Heikoop, J. M., Scott, D. B., Risk, M. J., Guilderson, T. P., and McKinney, R. A.: Stable isotopic composition of deep-sea gorgonian corals Primnoa spp.: a new archive of surface processes, Mar. Ecol. Prog. Ser., 301, 135–148, https://doi.org/10.3354/meps301135, 2005.

Sherwood, O. A., Jamieson, R. E., Edinger, E. N., and Wareham, V. E.: Stable C and N isotopic composition of cold-water corals from the Newfoundland and Labrador continental slope: Examination of trophic, depth and spatial effects, Deep-Sea Res. Pt. I, 55, 1392–1402, https://doi.org/10.1016/j.dsr.2008.05.013, 2008.

Sherwood, O. A., Davin, S. H., Lehmann, N., Buchwald, C., Edinger, E. N., Lehmann, M. F., and Kienast, M.: Stable isotope ratios in seawater nitrate reflect the influence of Pacific water along the northwest Atlantic margin, Biogeosciences, 18, 4491–4510, https://doi.org/10.5194/bg-18-4491-2021, 2021.

Shimeta, J. and Jumars, P. A.: Physical mechanisms and rates of particle capture by suspension feeders, Oceanogr. Mar. Biol., ISSN 0078-3218, 191–257, 1991.

Shumway, R. H., Stoffer, D. S., and Stoffer, D. S.: Time series analysis and its applications, Springer, https://doi.org/10.1007/978-3-319-52452-8, 2000.

Sigman, D. M., Karsh, K. L., and Casciotti, K. L.: Nitrogen Isotopes in the Ocean, in: Encyclopedia of Ocean Sciences, Elsevier Ltd, 40–54, https://doi.org/10.1016/B978-012374473-9.00632-9, 2009.

signal developers: signal: Signal processing, CRAN [code], https://CRAN.R-project.org/package=signal, last access: 1 December 2023.

St. Laurent, L., Stringer, S., Garrett, C., and Perrault-Joncas, D.: The generation of internal tides at abrupt topography, Deep-Sea Res. Pt. I, 50, 987–1003, https://doi.org/10.1016/S0967-0637(03)00096-7, 2003.

Stoffer, D.: astsa: Applied Statistical Time Series Analysis, CRAN [code], https://doi.org/10.32614/CRAN.package.astsa, 2020.

Straneo, F. and Saucier, F.: The outflow from Hudson Strait and its contribution to the Labrador Current, Deep-Sea Res. Pt. I, 55, 926–946, https://doi.org/10.1016/j.dsr.2008.03.012, 2008.

Sutcliffe Jr., W. H., Loucks, R. H., Drinkwater, K. F., and Coote, A. R.: Nutrient Flux onto the Labrador Shelf from Hudson Strait and its Biological Consequences, Can. J. Fish. Aquat. Sci., 40, 1692–1701, https://doi.org/10.1139/f83-196, 1983.

Thomson, D. H.: Marine Benthos in the Eastern Canadian High Arctic: Multivariate Analyses of Standing Crop and Community Structure, Arctic, 35, 61–74, 1982.

Tremblay, J.-É., Gratton, Y., Carmack, E. C., Payne, C. D., and Price, N. M.: Impact of the large-scale Arctic circulation and the North Water Polynya on nutrient inventories in Baffin Bay, J. Geophys. Res.-Oceans, 107, 26-1–26-14, https://doi.org/10.1029/2000JC000595, 2002.

Turner, J. T.: Zooplankton fecal pellets, marine snow, phytodetritus and the ocean's biological pump, Prog. Oceanogr., 130, 205–248, https://doi.org/10.1016/j.pocean.2014.08.005, 2015.

Vacelet, J. and Donadey, C.: Electron microscope study of the association between some sponges and bacteria, J. Exp. Mar. Biol. Ecol., 30, 301–314, https://doi.org/10.1016/0022-0981(77)90038-7, 1977.

Vander Zanden, M. J. and Rasmussen, J. B.: Variation in δ^{15}N and δ^{13}C trophic fractionation: Implications for aquatic food web studies, Limnol. Oceanogr., 46, 2061–2066, https://doi.org/10.4319/lo.2001.46.8.2061, 2001.

van der Kaaden, A.-S., van Oevelen, D., Mohn, C., Soetaert, K., Rietkerk, M., van de Koppel, J., and Gerkema, T.: Resemblance of the global depth distribution of internal-tide generation and cold-water coral occurrences, Ocean Sci., 20, 569–587, https://doi.org/10.5194/os-20-569-2024, 2024.

van Duyl, F., Hegeman, J., Hoogstraten, A., and Maier, C.: Dissolved carbon fixation by sponge–microbe consortia of deep water coral mounds in the northeastern Atlantic Ocean, Mar. Ecol. Prog. Ser., 358, 137–150, https://doi.org/10.3354/meps07370, 2008.

van Duyl, F. C., Lengger, S. K., Schouten, S., Lundälv, T., van Oevelen, D., and Müller, C. E.: Dark CO_2 fixation into phospholipid-derived fatty acids by the cold-water coral associated sponge *Hymedesmia* (*Stylopus*) *coriacea* (Tisler Reef, NE Skagerrak), Mar. Biol. Res., 1–17, https://doi.org/10.1080/17451000.2019.1704019, 2020.

Vaughan, D. and Dancho, M.: tibbletime: Time Aware Tibbles, CRAN [code], https://doi.org/10.32614/CRAN.package.tibbletime, 2020.

Vieira, R. P., Bett, B. J., Jones, D. O. B., Durden, J. M., Morris, K. J., Cunha, M. R., Trueman, C. N., and Ruhl, H. A.: Deep-sea sponge aggregations (Pheronema carpenteri) in the Porcupine Seabight (NE Atlantic) potentially degraded by demersal fishing, Prog. Oceanogr., 183, 102189, https://doi.org/10.1016/j.pocean.2019.102189, 2020.

Vogel, S.: Current-induced flow through living sponges in nature, P. Natl. Acad. Sci. USA, 74, 2069–2071, https://doi.org/10.1073/pnas.74.5.2069, 1977.

White, M.: Comparison of near seabed currents at two locations in the Porcupine Sea Bight–implications for benthic fauna, J. Mar. Biol. Assoc. UK, 83, 683–686, https://doi.org/10.1017/S0025315403007641h, 2003.

Whitney, F., Conway, K., Thomson, R., Barrie, V., Krautter, M., and Mungov, G.: Oceanographic habitat of sponge reefs on the Western Canadian Continental Shelf, Cont. Shelf Res., 25, 211–226, https://doi.org/10.1016/j.csr.2004.09.003, 2005.

Wickham, H.: Reshaping Data with the reshape Package, J. Stat. Softw., 21, 1–20, 2007.

Wickham, H.: ggplot2: Elegant Graphics for Data Analysis, Springer-Verlag New York, https://doi.org/10.1007/978-0-387-98141-3, 2016.

Wickham, H. and Bryan, J.: readxl: Read Excel Files, CRAN [code], https://doi.org/10.32614/CRAN.package.readxl, 2019.

Wilkinson, C. R., Garrone, R., Vacelet, J., and Smith, D. C.: Marine sponges discriminate between food bacteria and bacterial symbionts: electron microscope radioautography and in situ evidence, P. Roy. Soc. Lond. B, 220, 519–528, https://doi.org/10.1098/rspb.1984.0018, 1984.

Witte, U., Brattegard, T., Graf, G., and Springer, B.: Particle capture and deposition by deep-sea sponges from the Norwegian-Greenland Sea, Mar. Ecol. Prog. Ser., 154, 241–252, https://doi.org/10.3354/meps154241, 1997.

Wu, Y., Peterson, I. K., Tang, C. C. L., Platt, T., Sathyendranath, S., and Fuentes-Yaco, C.: The impact of sea ice on the initiation of the spring bloom on the Newfoundland and Labrador Shelves, J. Plankton Res., 29, 509–514, https://doi.org/10.1093/plankt/fbm035, 2007.

Wurz, E., Beazley, L., MacDonald, B., Kenchington, E., Rapp, H. T., and Osinga, R.: The Hexactinellid Deep-Water Sponge Vazella pourtalesii (Schmidt, 1870) (Rossellidae) Copes With Temporarily Elevated Concentrations of Suspended Natural Sediment, Front. Mar. Sci., 8, https://doi.org/10.3389/fmars.2021.611539, 2021.

Xie, Y.: knitr: A General-Purpose Package for Dynamic Report Generation in R, https://doi.org/10.32614/CRAN.package.knitr, 2020.

Yahel, G., Whitney, F., Reiswig, H. M., Eerkes-Medrano, D. I., and Leys, S. P.: In situ feeding and metabolism of glass sponges (Hexactinellida, Porifera) studied in a deep temperate fjord with a remotely operated submersible, Limnol. Oceanogr., 52, 428–440, https://doi.org/10.4319/lo.2007.52.1.0428, 2007.

Yashayaev, I.: Hydrographic changes in the Labrador Sea, 1960–2005, Prog. Oceanogr., 73, 242–276, https://doi.org/10.1016/j.pocean.2007.04.015, 2007.

Yashayaev, I.: Intensification and shutdown of deep convection in the Labrador Sea were caused by changes in atmospheric and freshwater dynamics, Commun. Earth Environ., 5, 1–23, https://doi.org/10.1038/s43247-024-01296-9, 2024.

Yashayaev, I. and Loder, J. W.: Further intensification of deep convection in the Labrador Sea in 2016, Geophys. Res. Lett., 44, 1429–1438, https://doi.org/10.1002/2016GL071668, 2017.